9114
NACA TN 2752

TECH LIBRARY KAFB, NM
0065914

NATIONAL ADVISORY COMMITTEE FOR AERONAUTICS

TECHNICAL NOTE 2752

A STUDY OF THE STABILITY OF THE LAMINAR BOUNDARY LAYER AS AFFECTED BY CHANGES IN THE BOUNDARY-LAYER THICKNESS IN REGIONS OF PRESSURE GRADIENT AND FLOW THROUGH THE SURFACE

By Neal Tetervin and David A. Levine

Langley Aeronautical Laboratory
Langley Field, Va.

Washington
August 1952

AFMDC
TECHNICAL LIBRARY
AFL 2811

TECH LIBRARY KAFB, NM

0065914

.A

NATIONAL ADVISORY COMMITTEE FOR AERONAUTICS

TECHNICAL NOTE 2752

A STUDY OF THE STABILITY OF THE LAMINAR BOUNDARY LAYER AS AFFECTED BY CHANGES IN THE BOUNDARY-LAYER THICKNESS IN REGIONS OF PRESSURE GRADIENT AND FLOW THROUGH THE SURFACE

By Neal Tetervin and David A. Levine

SUMMARY

The Schlichting method for the computation of the laminar boundary layer states that on an impervious surface the shape of the velocity profile is determined by the local effective pressure gradient; this gradient is directly proportional to the product of the actual pressure gradient and the square of the boundary-layer thickness. It is apparent, therefore, that in a region of falling pressure the Schlichting method predicts that an increase in boundary-layer thickness increases the effective pressure gradient and thus results in a more convex velocity profile. Because the increase in convexity is known to imply an increase in the critical boundary-layer Reynolds number, it would appear that an increase in boundary-layer thickness could increase the local critical Reynolds number more than the local boundary-layer Reynolds number.

In order to investigate this possibility, computations have been made by combining the Schlichting method with the Lin method for the calculation of the critical Reynolds number of a velocity profile. The computations indicate that in a region of falling pressure on an impervious surface an increase in boundary-layer thickness can cause the velocity profile shape to be changed enough by the increase in effective pressure gradient so that the ratio of the local critical Reynolds number to the local boundary-layer Reynolds number is increased. It thus appears that the local stability of the boundary layer can be increased by a local increase in boundary-layer thickness. The computations also indicate that similar effects occur when there is flow through the surface; in this case the results depend on the effective flow through the surface as well as on the effective pressure gradient.

These calculations suggest that an increase in boundary-layer thickness can decrease the disturbing effect of roughness particles without a decrease in stability. This conclusion is implied by the result that an increase in boundary-layer thickness reduces the velocity at a fixed distance from the surface more than the change in velocity profile increases the velocity. One method of increasing the boundary-layer thickness, namely, blowing near the stagnation point, has been investigated theoretically and seems to have limited potentialities because the blowing produces a significant increase in boundary-layer thickness only over the foremost portion of the airfoil.

INTRODUCTION

A number of years ago investigators noticed that a falling pressure in the direction of flow was able to increase the extent of laminar flow on a surface and thereby decrease its friction drag (references 1, 2, and 3). This observation was made the basis for the design of airfoils that are able to have much smaller drag coefficients than previously known airfoils. In order to obtain the small drag coefficients, however, it is necessary that the airfoil surface be smooth and free of waves. The requirement of a smooth and wave-free surface has, to the present, prevented the consistent attainment in flight of wing drag coefficients as small as those obtained in wind-tunnel tests.

The experimental finding that under proper conditions a falling pressure in the direction of flow causes increases in the extent of laminar flow was given a theoretical basis by the work of reference 4. The theoretical work showed that a pressure drop increases the convexity of velocity profiles and thereby increases their critical Reynolds numbers. The critical Reynolds number is the Reynolds number below which transition to turbulent flow cannot be caused by the growth of small departures from the mean velocity inside the boundary layer as the fluid moves downstream. To form the Reynolds number the velocity at the outer edge of the boundary layer is used; the length is a boundary-layer thickness.

Another important theoretical finding (reference 5) was that a flow of fluid into the surface increases the convexity of the velocity profile and thereby increases its critical Reynolds number; an outflow was found to decrease the critical Reynolds number. Because the effects on the critical Reynolds number are large for very small flow velocities through the surface, the method of maintaining laminar flow by sucking fluid into the airfoil through a porous surface appeared to have practical value. In order to test the method, the work of reference 6 was done. Full-chord laminar flow was observed up to a Reynolds number of 20×10^6 and it was concluded that larger Reynolds numbers would not limit the extent of laminar flow if the surface were sufficiently smooth and free of waviness.

Another method for maintaining laminar flow was based on the experimental observation that transition often seems to occur at a fairly definite value of the boundary-layer Reynolds number. Examples of the application of this observation are references 7, 8, and 9 in which a number of slots were placed along the airfoil surface and air drawn into the interior in order to decrease the boundary-layer Reynolds number.

In tests of each of the three methods, namely, pressure drop, suction through a porous surface, and limitation of magnitude of boundary-layer Reynolds number, it was found that, in order to avoid early transition to turbulent flow, the surface has to be free of noticeable roughness particles and other departures from smoothness. The work of reference 10 indicated that the roughness Reynolds number, formed from the height of the roughness particle and the velocity at a distance from the surface equal to the roughness height with the particle absent, furnishes a

measure of the disturbing effect of a particle. For a small effect, a small roughness Reynolds number is necessary. All three methods for keeping the boundary layer laminar, however, increase rather than decrease the roughness Reynolds number of a particle.

In the Schlichting method (reference 11), the shape of the velocity profile on an impervious surface depends only on the kinematic viscosity, on the local gradient of velocity at the outer edge of the boundary layer, and on the local boundary-layer thickness. The combination of variables is such that an increase in boundary-layer thickness increases the effect of velocity gradient; therefore, in a region of falling pressure, an increase in boundary-layer thickness results in a more convex velocity profile. Because the increase in convexity carries with it an increase in the critical boundary-layer Reynolds number, the possibility arises that an increase in boundary-layer thickness may increase the local critical Reynolds number more than the local boundary-layer Reynolds number is increased by the increase in thickness. There is thus the possibility that an increase in boundary-layer thickness can increase the stability of the boundary layer.

The purpose of the present work is therefore to investigate theoretically the effect of an increase in boundary-layer thickness on the stability of the boundary layer. The analysis also includes an investigation of the effect of an increase in boundary-layer thickness on the roughness Reynolds number and of the ability of blowing at the stagnation point to increase the boundary-layer thickness without making the boundary layer unstable.

SYMBOLS

a,b coefficients in expression for ψ

$$C_o = \left(\frac{k_1}{\sqrt{k}}\right)_s = \left(-v_w\sqrt{\frac{R_c}{\frac{dU}{dx}}}\right)_s$$

C_{D_P} drag equivalent of power required for boundary-layer control

C_{D_t} sum of wake drag coefficient and C_{D_P}

$$C_Q = \frac{\oint \bar{v}_w \, d\bar{x}}{\bar{U}_o \bar{c}}$$

$\bar{c}$ chord of airfoil

c_o,c_1,c_2 coefficients in expression for g

E_B efficiency of boundary-layer control system

E_P efficiency of aircraft propulsive system

$$f = \frac{\bar{\tau}_w \bar{\theta}}{\bar{\mu}\bar{U}}$$

$$f_1 = -\frac{\bar{v}_w}{\bar{U}_o}\sqrt{\frac{\bar{U}_o \bar{c}}{\bar{\nu}}}$$

$$F_1 = 1 - e^{-\eta}$$

$$F_2 = 1 - e^{-\eta} - \sin\frac{\pi}{6}\eta \qquad (0 < \eta \leqq 3)$$

$$= -e^{-\eta} \qquad (\eta \geqq 3)$$

F function of y

$$g = \frac{\bar{\theta}}{\bar{\delta}_1} = c_o + c_1 K + c_2 K^2$$

$$G = 2\left[f - k\left(2 + \frac{\delta^*}{\theta}\right) - k_1\right]$$

$\bar{h}$ height of roughness particle

$\bar{H}$ total pressure

$$J = \frac{v_w^2 R_c}{2\frac{dU}{dx}} = \frac{f_1^2}{2\frac{dU}{dx}} = \frac{k_1^2}{2k}$$

K velocity-profile shape parameter

$$p = \frac{\bar{p} - \bar{p}_o}{\bar{\rho}_o \bar{U}_o^2}$$

$\bar{p}$ static pressure

$\bar{p}_o$ free-stream static pressure

P power required for boundary-layer control

$\bar{Q}$ volume flow per unit time

$\bar{q}_o = \frac{\bar{\rho}_o \bar{U}_o^2}{2}$

R_{θ_c} critical Reynolds number, value of R_θ at which a small disturbance is neither damped nor amplified

$R_\theta = \frac{\overline{\theta U}}{\bar{\nu}}$

$R_{\delta^*_c}$ critical Reynolds number, value of R_{δ^*} at which a small disturbance is neither damped nor amplified

$R_{\delta^*} = \frac{\bar{\delta}^* \bar{U}}{\bar{\nu}}$

R_h roughness Reynolds number $\left(\frac{\bar{u}_h \bar{h}}{\bar{\nu}}\right)$

R_c airfoil Reynolds number $\left(\frac{\bar{U}_o \bar{c}}{\bar{\nu}}\right)$

$\bar{U}$ velocity at outer edge of boundary layer

$\bar{u}$ velocity in direction of $\bar{x}$

$u = \frac{\bar{u}}{\bar{U}_o}$

$U = \frac{\bar{U}}{\bar{U}_o}$

$\bar{U}_o$ free-stream velocity

$\bar{u}_h$ velocity at $\bar{y} = \bar{h}$ with roughness particle absent

$\bar{v}_w$ velocity through surface, positive outward

$v_w = \frac{\bar{v}_w}{\bar{U}_o}$

$v = \frac{\bar{v}}{\bar{U}_o}$

$\bar{v}$ velocity normal to surface, positive outward

$\bar{V}$ velocity in direction of $\bar{y}$-axis, stagnation-point flow

$V = \frac{\bar{V}}{\bar{U}_o}$

$\bar{x}$ distance along surface measured from stagnation point

$x = \frac{\bar{x}}{\bar{c}}$

Δx increment in x

$\bar{y}$ distance normal to surface, positive outward

$y = \frac{\bar{y}}{\bar{c}}$

$Z = \theta^2 R_c$

α angle of attack

$\bar{\delta}_1$ measure of boundary-layer thickness

δ^* displacement thickness $\left(\int_0^\infty \left(1 - \frac{u}{U}\right) dy\right)$

$\eta = \frac{\bar{y}}{\bar{\delta}_1}$

θ momentum thickness $\left(\int_0^\infty \frac{u}{U}\left(1 - \frac{u}{U}\right)dy\right)$

$$k = \frac{\bar{\theta}^2}{\bar{\nu}} \frac{d\bar{U}}{d\bar{x}} = \frac{R_\theta{}^2}{R_c}\left(\frac{1}{U^2} \frac{dU}{dx}\right) = Z \frac{dU}{dx}$$

$$k_1 = - \frac{\bar{v}_w\bar{\theta}}{\bar{\nu}} = - \frac{v_w}{U} R_\theta = f_1\sqrt{Z}$$

$$\lambda = \frac{\bar{\delta}_1{}^2}{\bar{\nu}} \frac{d\bar{U}}{d\bar{x}}$$

$$\lambda_1 = - \frac{\bar{v}_w\bar{\delta}_1}{\bar{\nu}}$$

$\bar{\mu}$ viscosity of fluid

$\bar{\nu}$ kinematic viscosity of fluid $(\bar{\mu}/\bar{\rho})$

$\bar{\rho}_o$ free-stream density

$\bar{\rho}$ density of fluid

$\bar{\tau}_w$ surface shearing stress

ϕ function of y

ψ nondimensional stream function $\left(\frac{\bar{\Psi}}{\bar{U}_o\bar{c}}\right)$

$\bar{\psi}$ stream function

Subscripts:

s stagnation point

w at surface

∞ far behind wing

x at station x

$x+\Delta x$ at station $x + \Delta x$

Barred quantities are dimensional.

ANALYSIS

Effect of an increase in boundary-layer thickness on the stability of the laminar boundary layer.- The analysis makes use of a modification of Schlichting's method for the calculation of laminar-boundary-layer velocity profiles (reference 11). The modification consists in using the boundary-layer momentum thickness $\bar{\theta}$ as the reference length instead of the length $\bar{\delta}_1$ used by Schlichting. The use of $\bar{\theta}$ instead of $\bar{\delta}_1$ eliminates two auxiliary parameters, λ and λ_1, and makes the extension of the Schlichting method to cases of uniformly distributed blowing relatively simple. The modified Schlichting method is described in appendix A.

From the definition of the critical Reynolds number (reference 12) it follows that the boundary layer is unstable when the ratio of the local critical Reynolds number to the local boundary-layer Reynolds number $\frac{R_{\theta_c}}{R_\theta}$ is less than unity, neutrally stable when $\frac{R_{\theta_c}}{R_\theta} = 1$, and stable when $\frac{R_{\theta_c}}{R_\theta} > 1$. In the present work the assumption is made that the numerical value of the ratio $\frac{R_{\theta_c}}{R_\theta}$ at a distance x from the stagnation point is a measure of the stability of the boundary layer at that value of x. It is assumed that the boundary layer becomes more stable as the ratio $\frac{R_{\theta_c}}{R_\theta}$ increases. (In this analysis it is more convenient to use R_{θ_c} and R_θ than R_{δ^*} and $R_{\delta^*_c}$.)

A conclusion of reference 13 is that the critical Reynolds number R_{θ_c} depends only on the shape of the velocity profile. In the Schlichting method all velocity profiles are a single-parameter family. Therefore to each value of K, the velocity-profile parameter, there corresponds a value of R_{θ_c}; that is,

$$R_{\theta_c} = R_{\theta_c}(K) \tag{1}$$

The function $R_{\theta_c}(K)$ was calculated by Lin's rapid method (reference 12) and is shown in figure 1. (See also reference 6.)

The possibility that an increase in $\overline{\theta}$ can increase K enough to cause a larger increase in R_{θ_c} than in R_θ is now investigated. The investigation is made for the general case $v_w \neq 0$; $v_w = 0$ is then a special case.

In order to determine the effect on $\frac{R_{\theta_c}}{R_\theta}$ at a specific value of x of an increase in $\overline{\theta}$ at that value of x with $\overline{\nu}$, $\overline{U}$, $\frac{d\overline{U}}{d\overline{x}}$, and $\overline{v}_w$ fixed $\left(R_c,\ U,\ \frac{dU}{dx}, \text{ and } v_w \text{ fixed}\right)$, it is convenient to obtain $\frac{R_{\theta_c}}{R_\theta}$ as a function of the parameters K and $\frac{v_w{}^2 R_c}{2\frac{dU}{dx}}$. The shape parameter K is a function of the two quantities k and k_1 defined by:

$$k = \frac{\overline{\theta}^2}{\overline{\nu}} \frac{d\overline{U}}{d\overline{x}}$$

and

$$k_1 = -\frac{\overline{v}_w \overline{\theta}}{\overline{\nu}}$$

These definitions can also be written as:

$$k = \frac{R_\theta{}^2}{R_c} \frac{1}{U^2} \frac{dU}{dx} \tag{2}$$

and

$$k_1 = -\frac{v_w}{U} R_\theta \tag{3}$$

When the definitions for k and k_1 are substituted into the following equation connecting K, k, and k_1 (equation (A8), appendix A):

$$g^2(K + 1) - fk_1 - k = 0 \tag{4}$$

the result is

$$\frac{R_\theta^2}{R_c} \frac{1}{U^2} \frac{dU}{dx} - f \frac{v_w}{U} R_\theta - g^2(K + 1) = 0 \tag{5}$$

The quantities f and g where

$$f = \frac{\bar{\tau}_w \bar{\theta}}{\bar{\mu}\bar{U}}$$

and

$$g = \frac{\bar{\theta}}{\bar{\delta}_1}$$

are functions of K alone. Equation (5) is solved for R_θ; the result is

$$\frac{v_w}{U} R_\theta = Jf\left[1 \pm \sqrt{1 + \frac{2g^2(K + 1)}{Jf^2}}\right] \tag{6}$$

where

$$J = \frac{v_w^2 R_c}{2 \frac{dU}{dx}} = \frac{f_1^2}{2 \frac{dU}{dx}} = \frac{k_1^2}{2k}$$

It is noted that the parameter J is independent of R_θ and therefore does not change when $\overline{\theta}$ at a fixed value of x is changed.

The sign of the radical in equation (6) is determined by the fact that R_θ is always positive. The sign is given in the following table:

J	K + 1	Sign
$\frac{v_w}{U} > 0$		
>0	$\geqq 0$	+
>0	$\leqq 0$	±
<0	<0	-
$\frac{v_w}{U} < 0$		
>0	>0	-
<0	$\leqq 0$	+
<0	$\geqq 0$	±

By combining equations (1) and (6) the following result is obtained:

$$\frac{R_{\theta_c}}{\frac{v_w}{U} R_\theta} = \frac{R_{\theta_c}(K)}{Jf\left[1 \pm \sqrt{1 + \frac{2g^2(K + 1)}{Jf^2}}\right]} \qquad (v_w \neq 0) \tag{7}$$

Equation (7) fixes $\frac{R_{\theta_c}}{R_\theta}$ when $\frac{v_w}{U}$, J, and K are known. The variation of $\frac{R_{\theta_c}}{\frac{v_w}{U} R_\theta}$ with K for constant values of J is shown in figure 2.

(The curves of fig. 2 have been numbered; the value of J to which the numbers correspond may be obtained from table I.)

Usually the airfoil does not have a porous surface; in this case $v_w = 0$ and equation (7) is replaced by

$$\frac{R_{\theta_c}}{R_\theta}\sqrt{\frac{U^2R_c}{\left|\frac{dU}{dx}\right|}} = \frac{R_{\theta_c}(K)}{g\sqrt{|1 + K|}} \qquad \left(\frac{dU}{dx} \neq 0\right) \tag{8}$$

Equation (8) can be obtained either by putting $v_w = 0$ in equation (5), solving for R_θ, and combining with equation (1), or by taking the limit as $v_w \rightarrow 0$ in equation (7). The function $\frac{R_{\theta_c}}{R_\theta}\sqrt{\frac{U^2R_c}{\left|\frac{dU}{dx}\right|}}$ is shown in figure 3.

The quantity under the square-root sign in equation (6) must be positive; thus,

$$1 + \frac{2g^2(K + 1)}{Jf^2} \geqq 0$$

When the equality sign is used, the result is the curve defined by the equation

$$\frac{R_{\theta_c}}{\frac{v_w}{U}R_\theta} = -\frac{R_{\theta_c}(K)}{\frac{2g^2(K + 1)}{f}} \tag{9}$$

and shown by dashed lines in figures 2(a) and 2(b). A curve of $\frac{R_{\theta_c}}{\frac{v_w}{U}R_\theta}$ for a fixed value of J cannot cross the dashed curve.

Although the relation between K, k, and k_1 (equation (4) and fig. 4) is used in obtaining equations (7) and (8), not all combinations of values are allowable because some correspond to a physically unrealizable behavior of the boundary layer. Thus, in order to avoid the contradiction that, at a fixed value of k_1 and with k negative $\left(\frac{dU}{dx} < 0\right)$, an increase in k $\left(\text{a decrease in the magnitude of } \frac{dU}{dx} \text{ for } \frac{dU}{dx} < 0\right)$ can result in separation, only the portion of the curves for K, k, and k_1 in figure 4(a) for which $\left(\frac{\partial K}{\partial k}\right)_{k_1} \geqq 0$ is used. The boundary curve, shown as a dashed line in figure 4(a), passes through the points at which $\left(\frac{\partial K}{\partial k}\right)_{k_1}$ changes from ∞ to $-\infty$. Its equation is obtained by applying the condition

$$\infty \geqq \left(\frac{\partial K}{\partial k}\right)_{k_1} \geqq 0$$

to the expression,

$$\left(\frac{\partial K}{\partial k}\right)_{k_1} = \frac{1}{\frac{df}{dK}\left[\frac{\frac{dg^2(K + 1)}{dK}}{\frac{df}{dK}} - k_1\right]} \tag{10}$$

obtained from equation (4). The subscript on the partial derivative denotes the quantity held constant during the differentiation. From equation (10), the fact that $\frac{df}{dK} > 0$, and the inequality for $\left(\frac{\partial K}{\partial k}\right)_{k_1}$, the result is obtained that:

$$k_1 \leqq \frac{\frac{dg^2(K + 1)}{dK}}{\frac{df}{dK}}$$

On the boundary curve the equality sign applies. When the condition

$$k_1 = \frac{\dfrac{dg^2(K + 1)}{dK}}{\dfrac{df}{dK}}$$

is used with equation (4), the equation of the boundary curve is found to be

$$k = g^2(K + 1) - f \frac{\dfrac{dg^2(K + 1)}{dK}}{\dfrac{df}{dK}} \tag{11}$$

All physically meaningful values of k and K lie to the right of the dashed boundary curve (fig. 4(a)). For $k_1 = 0$ (that is, $v_w = 0$) only values of K greater than -1.913 are allowable.

The curves of $\dfrac{R_{\theta_c}}{\dfrac{v_w}{U} R_\theta}$ in figure 2 thus satisfy the conditions that

$$R_\theta > 0$$

$$1 + \frac{2g^2(K + 1)}{Jf^2} \geqq 0$$

and

$$\left(\frac{\partial K}{\partial k}\right)_{k_1} \geqq 0$$

The curve of $\frac{R_{\theta_c}}{R_\theta}\sqrt{\frac{U^2R_c}{\left|\frac{dU}{dx}\right|}}$ (fig. 3) satisfies the conditions that:

$R_\theta > 0$ and $\left(\frac{\partial K}{\partial k}\right)_{k_1} \geqq 0$.

Before the effect of an increase in $\overline{\theta}$ on the ratio $\frac{R_{\theta_c}}{R_\theta}$ can be found from figures 2 and 3, the effect of the increase in $\overline{\theta}$ on K must be found. The sign of the derivative $\frac{\partial K}{\partial R_\theta}$ is thus required. Only $\overline{\theta}$ varies; therefore, R_θ varies, but R_c, U, $\frac{dU}{dx}$, and v_w do not. From equation (4) $K = K(k,k_1)$; therefore,

$$\frac{\partial K}{\partial R_\theta} = \left(\frac{\partial K}{\partial k}\right)_{k_1} \frac{\partial k}{\partial R_\theta} + \left(\frac{\partial K}{\partial k_1}\right)_k \frac{\partial k_1}{\partial R_\theta}$$

where the subscripts denote the quantity held constant. Now from equation (2)

$$R_\theta \frac{\partial k}{\partial R_\theta} = 2k$$

and from equation (3)

$$R_\theta \frac{\partial k_1}{\partial R_\theta} = k_1$$

Therefore,

$$R_\theta \frac{\partial K}{\partial R_\theta} = 2k\left(\frac{\partial K}{\partial k}\right)_{k_1} + k_1\left(\frac{\partial K}{\partial k_1}\right)_k \tag{12}$$

From equation (4) there follows

$$\left(\frac{\partial K}{\partial k}\right)_{k_1} = \frac{1}{\frac{dg^2(K + 1)}{dK} - \frac{df}{dK} k_1}$$

and

$$\left(\frac{\partial K}{\partial k_1}\right)_k = \frac{f}{\frac{dg^2(K + 1)}{dK} - \frac{df}{dK} k_1}$$

When these expressions for $\left(\frac{\partial K}{\partial k}\right)_{k_1}$ and $\left(\frac{\partial K}{\partial k_1}\right)_k$ are substituted into equation (12), the result is

$$R_\theta \frac{\partial K}{\partial R_\theta} = \frac{2g^2(K + 1) - k_1 f}{\frac{dg^2(K + 1)}{dK} - k_1 \frac{df}{dK}} \tag{13}$$

The curves in figure 2 are identified by the value of the parameter J. (See table I.) Therefore, in order to find the sign of $\frac{\partial K}{\partial R_\theta}$

for any curve in figure 2, it is necessary to introduce the parameter J into equation (13) for $R_\theta \frac{\partial K}{\partial R_\theta}$. Equation (6) is used to obtain:

$$k_1 = -\frac{v_w}{U} R_\theta = -Jf\left[1 \pm \sqrt{1 + \frac{2g^2(K + 1)}{Jf^2}}\right]$$

Equation (13) thus becomes:

$$R_\theta \frac{\partial K}{\partial R_\theta} = \frac{2g^2(K + 1) + f^2J\left[1 \pm \sqrt{1 + \frac{2g^2(K + 1)}{Jf^2}}\right]}{\frac{dg^2(K + 1)}{dK} + \frac{df}{dK} fJ\left[1 \pm \sqrt{1 + \frac{2g^2(K + 1)}{Jf^2}}\right]} \tag{14}$$

The quantity $R_\theta \frac{\partial K}{\partial R_\theta}$ is plotted against K for constant values of J in figure 5(a) for $v_w > 0$ and in figure 5(b) for $v_w < 0$. The curves of $R_\theta \frac{\partial K}{\partial R_\theta}$ against K also satisfy the conditions that

$$R_\theta > 0$$

$$1 + \frac{2g^2(K + 1)}{Jf^2} \geqq 0$$

and

$$\left(\frac{\partial K}{\partial k}\right)_{k_1} \geqq 0$$

When $1 + \frac{2g^2(K + 1)}{Jf^2} = 0$, the numerator of equation (14) is zero; then, $R_\theta \frac{\partial K}{\partial R_\theta} = 0$.

The curve of $R_\theta \frac{\partial K}{\partial R_\theta}$ against K for $v_w = 0$, calculated from equation (14) with $J = 0$, is shown in figure 6. This curve satisfies the conditions that $R_\theta > 0$ and $\left(\frac{\partial K}{\partial k}\right)_{k_1} \geqq 0$.

Now consider figures 3 and 6 which are for $v_w = 0$. It is apparent from figure 6 that when $v_w = 0$ an increase in R_θ decreases K if $K < -1$, does not change K if K is initially equal to -1, and increases K if $K > -1$. Therefore an increase in $\bar{\theta}$, and thus in R_θ, causes $\frac{R_{\theta_c}}{R_\theta}$ to increase if $K > -0.925$ (fig. 3). Consequently, an increase in boundary-layer thickness increases rather than decreases the stability of the boundary layer if $K > -0.925$. When $K < -0.925$ a small increase in boundary-layer thickness decreases the stability of the boundary layer; conversely, when $K < -0.925$ a small decrease in thickness increases the stability.

For $K > -1$ and $v_w = 0$, the pressure falls along the surface in the direction of flow; when $K < -1$ and $v_w = 0$, the pressure rises in the direction of flow (equation (4)). The values $K = -1$ and $v_w = 0$ correspond to a flow with zero pressure gradient.

Figures 2(a) and 5(a) (for $v_w > 0$) indicate that when $R_\theta \frac{\partial K}{\partial R_\theta} < 0$ (curves 6 to 13 inclusive) an increase in R_θ decreases the stability. When $R_\theta \frac{\partial K}{\partial R_\theta} > 0$ (curves 1 to 5 inclusive), the stability may either be increased or decreased by an increase in R_θ depending on the values of K and J and the magnitude of the increase in R_θ.

For $v_w < 0$ the conclusion is similar to that for $v_w > 0$; namely, when $R_\theta \frac{\partial K}{\partial R_\theta} < 0$ (curves 9 to 11, figs. 2(b) and 5(b)) an increase in R_θ decreases the stability. When $R_\theta \frac{\partial K}{\partial R_\theta} > 0$ (curves 1 to 7 inclusive,

figs. 2(b) and 5(b)) the stability may either be increased or decreased by an increase in R_θ, depending on the values of K and J and the magnitude of the increase in R_θ. For curve 8 the stability is decreased by an increase in R_θ.

The computations thus indicate that under suitable conditions an increase in boundary-layer thickness can increase the stability of the laminar boundary layer.

Effect of an increase in boundary-layer thickness on the roughness Reynolds number R_h.- Because the disturbing effect of a roughness particle is decreased when its Reynolds number R_h is decreased sufficiently (reference 10), it is desirable to examine the effect on R_h of an increase in $\overline{\theta}$, that is, an increase in R_θ with R_c, U, $\frac{dU}{dx}$, and v_w fixed. Although an increase in boundary-layer thickness places the roughness particle at a smaller fraction of the boundary-layer thickness from the surface and consequently in a region of smaller velocity, the increase in thickness also changes the velocity profile and therefore the velocity at a fixed distance from the surface. Whether the increase in velocity associated with the change in velocity profile can be greater than the decrease in velocity caused by the increase in the boundary-layer thickness is now investigated.

The definition of R_h is

$$R_h = \frac{\overline{u}_h\overline{h}}{\overline{\nu}} \tag{15}$$

Although the assumption of reference 10 that

$$\overline{u}_h = \overline{h}\left(\frac{\partial\overline{u}}{\partial\overline{y}}\right)_w$$

becomes less accurate as the curvature of the velocity profile increases, it can be shown that this assumption overestimates the change in velocity caused by the change in velocity profile. The assumption is therefore retained in the present analysis. Therefore, equation (15) becomes

$$R_h = \frac{\overline{h}^2\left(\frac{\partial\overline{u}}{\partial\overline{y}}\right)_w}{\overline{\nu}}$$

but from reference 11

$$\left(\frac{\partial \bar{u}}{\partial \bar{y}}\right)_w = \frac{\bar{U}}{\bar{\theta}} f(K)$$

Therefore,

$$R_h = \frac{\bar{h}^2\bar{U}}{\bar{\theta}} \frac{f(K)}{\bar{\nu}}$$

or

$$R_h = \frac{h^2 R_c{}^2 U^2}{R_\theta} f(K) \tag{16}$$

Because $f(K)$ changes with R_θ, it is not obvious that an increase in R_θ always decreases R_h. The change in R_h caused by a change in R_θ alone, really $\bar{\theta}$ alone, is given by:

$$\frac{\partial R_h}{\partial R_\theta} = h^2 R_c{}^2 U^2 \left[\frac{f(K)}{-R_\theta{}^2} + \frac{1}{R_\theta} \frac{df(K)}{dK} \frac{\partial K}{\partial R_\theta}\right]$$

or

$$\frac{\partial R_h}{\partial R_\theta} = \frac{R_h}{R_\theta}\left(-1 + \frac{1}{f} \frac{df}{dK} R_\theta \frac{\partial K}{\partial R_\theta}\right)$$

When equation (13) for $R_\theta \frac{\partial K}{\partial R_\theta}$ is used, the result is:

$$\frac{R_\theta}{R_h}\frac{\partial R_h}{\partial R_\theta} = \frac{-\dfrac{\dfrac{dg^2(K+1)}{dK}}{df/dK} + \dfrac{2g^2(K+1)}{f}}{\dfrac{\dfrac{dg^2(K+1)}{dK}}{df/dK} - k_1} \tag{17}$$

The partial derivative $\frac{R_\theta}{R_h}\frac{\partial R_h}{\partial R_\theta}$ is shown in figure 7 as a function of K for four values of k_1. The partial derivative $\frac{\partial R_h}{\partial R_\theta}$ is always negative because the numerator of equation (17) is negative for all values of K and the denominator is positive for all values of K. That the denominator is positive follows from the condition that $\left(\frac{\partial K}{\partial k}\right)_{k_1} \geqq 0$; this requires that:

$$k_1 \leqq \frac{\dfrac{dg^2(K+1)}{dK}}{\dfrac{df}{dK}}$$

Therefore, an increase in R_θ always decreases R_h; that is, an increase in boundary-layer thickness reduces the velocity at a fixed distance from the surface more than the change in velocity profile increases the velocity. Consequently, a sufficient increase in boundary-layer thickness always decreases the disturbing effect of roughness particles.

Effect of an increase in boundary-layer thickness on the stability of the boundary layer of two typical airfoils.- The computations thus indicate that a sufficient increase in boundary-layer thickness can decrease the disturbing effect of roughness particles and that under suitable conditions an increase in boundary-layer thickness can increase the stability of the laminar boundary layer. An equivalent statement of these two results is that $\frac{\partial R_h}{\partial R_\theta}$ is always negative and that $\frac{\partial \frac{R_{\theta_c}}{R_\theta}}{\partial R_\theta}$ can be positive.

In order to determine whether typical airfoils with neither suction nor blowing have regions in which $\frac{\partial \frac{R_{\theta_c}}{R_\theta}}{\partial R_\theta} > 0$, that is, regions in which $K > -0.925$ (fig. 3), the modified Schlichting method was used to calculate the distribution of K along $\bar{x}$ for the NACA 64A010 and NACA 64_2A015 airfoil sections (reference 14) at zero angle of attack (figs. 8(a) and 9(a)). The distribution of K along x for $v_w = 0$ at all values of x is independent of R_c. For the NACA 64A010 airfoil section only the boundary layer over the forward $2\frac{1}{2}$ percent of the airfoil has $\frac{\partial \frac{R_{\theta_c}}{R_\theta}}{\partial R_\theta} > 0$. For the NACA 64_2A015 airfoil, however, $\frac{\partial \frac{R_{\theta_c}}{R_\theta}}{\partial R_\theta} > 0$ for the forward $22\frac{1}{2}$ percent of the surface. The region of $\frac{\partial \frac{R_{\theta_c}}{R_\theta}}{\partial R_\theta} > 0$ is greater for the NACA 64_2A015 airfoil section than for the NACA 64A010 airfoil section because the NACA 64_2A015 airfoil section has larger values of $\frac{dU}{dx}$ over its forward portion than the NACA 64A010 section. (Compare figs. 10 and 11.)

It is to be noted that figures 3 and 6 indicate that by a sufficient increase in boundary-layer thickness the boundary layer over the forward portions of both the NACA 64A010 and the NACA 64_2A015 airfoil sections can be made stable. This conclusion follows from the result that $\frac{\partial K}{\partial R_\theta} > 0$ for $K > -1$ (fig. 6) and the result that

$$\frac{d}{dK}\left(\frac{R_{\theta_c}}{R_\theta}\sqrt{\frac{U^2 R_c}{\left|\frac{dU}{dx}\right|}}\right) > 0$$

for $K > -0.925$ (fig. 3). A sufficient increase in R_θ (in $\bar{\theta}$) can therefore make $\frac{R_{\theta_c}}{R_\theta}$ equal unity unless $\frac{U^2 R_c}{\left|\frac{dU}{dx}\right|}$ is very large. For

example, if the value of θ at $x = 0.35$ on the NACA 64A010 airfoil at $R_c = 10^7$ is multiplied by 3.45, the value of R_θ is increased from 1221 to 4208 and the value of $\frac{R_{\theta_c}}{R_\theta}$ is increased from 0.239 to 1.0.

When $\frac{dU}{dx} = 0$, $K = -1$ and $\frac{R_{\theta_c}}{R_\theta}\sqrt{\frac{U^2 R_c}{\left|\frac{dU}{dx}\right|}} = \infty$. In this case, the flat-plate flow, an increase in R_θ can only make the boundary layer more unstable.

Effect of blowing at the stagnation point.- The analysis has shown that in a region of falling pressure on an airfoil having the usual type of surface ($v_w = 0$) the disturbing effect of roughness particles can be decreased and the stability of the boundary layer increased by an increase in boundary-layer thickness. This result suggests that an effort be made to find a method for increasing the boundary-layer thickness without causing transition. The second part of the analysis investigates such a method, namely, blowing in the region of the stagnation point.

The work of reference 15 (see also appendix B) has shown that even for large blowing velocities the velocity profile in a stagnation-point flow, a flow in which $U = \left(\frac{dU}{dx}\right)_s x$, does not have an inflection point for $y > 0$. In fact, as v_w becomes very large and positive (blowing) the velocity profile approaches the sine profile:

$$\frac{u}{U} = \sin\left(\frac{y}{v_w}\frac{dU}{dx}\right)$$

which has an inflection point at $y = 0$. The value of R_{θ_c} for this limiting velocity profile is 228 (appendix B). The value of R_{θ_c} at the stagnation point is therefore always greater than or equal to 228. At the stagnation point, however, $R_\theta = 0$. Therefore, R_{θ_c} is there always greater than R_θ with the result that blowing at and near the stagnation point can be used to thicken the boundary layer without making it immediately unstable.

It is shown in appendix C that the Von Kármán momentum equation upon which the Schlichting method is based is valid for a stagnation-point flow even when there are large velocities through the surface. The Schlichting method can therefore be used to calculate the development of the boundary layer near the stagnation point even when there are large velocities through the surface.

As a result, blowing in the region of the stagnation point was investigated for both the NACA 64A010 and the NACA 64_2A015 airfoil sections at $\alpha = 0^\circ$ and $R_c = 10^7$. The independent parameter was the quantity k which was given the values 0.709 and 7.09; these values are, respectively, 10 and 100 times the value of k at the stagnation point without blowing. Because

$$k = \frac{\bar{\theta}^2}{\bar{\nu}} \frac{d\bar{U}}{d\bar{x}}$$

the factors 10 and 100 mean that the value of $\bar{\theta}$ at the stagnation point is, respectively, $\sqrt{10}$ and 10 times the value of $\bar{\theta}$ for zero blowing. The values of k_1 and K are obtained from figure 12 and the chosen value of k. The magnitude of $(v_w)_s$ is obtained from figure 12 and the definition

$$C_o = \left(-v_w \sqrt{\frac{R_c}{\frac{dU}{dx}}}\right)_s$$

The behavior of the boundary layer is then computed by the modified Schlichting method (appendix A).

At $R_c = 10^7$, $\alpha = 0^\circ$, and $v_w = 0$ everywhere, the Reynolds number R_θ becomes larger than the critical Reynolds number R_{θ_c} at $x = 0.038$ for the NACA 64A010 airfoil section (fig. 8(b)) and at $x = 0.060$ for the NACA 64_2A015 airfoil section (fig. 9(b)). The boundary layer on both airfoils is thus unstable for the greater part of the region of falling pressure. When v_w is made positive (blowing) near the stagnation point, R_θ is increased and R_{θ_c} is decreased so that R_θ becomes equal to R_{θ_c} nearer the stagnation point than when

$v_w = 0$. The values of R_θ and R_{θ_c}, however, can then be made equal to one another for some distance by decreasing v_w along the surface in the proper manner. When v_w reaches zero, control of the boundary layer in the present examples ends. Of course the boundary layer can be made neutrally stable to the trailing edge by allowing v_w to be negative (suction) from the point where $v_w = 0$ to the trailing edge (see reference 6). In this case the boundary-layer thickness is first increased by the blowing and then decreased by the suction. The net effect depends on the value of x, the Reynolds number, the airfoil velocity distribution, and the magnitude of the blowing velocity at the stagnation point.

The distribution of v_w necessary to make $R_\theta = R_{\theta_c}$ is calculated by using the relation between R_θ and Z together with the requirement that $R_\theta = R_{\theta_c}$. The relation between R_θ and Z is

$$R_\theta = U\sqrt{Z}\sqrt{R_c}$$

but

$$R_\theta = R_{\theta_c}$$

therefore

$$R_{\theta_c} = U\sqrt{Z}\sqrt{R_c} \tag{18}$$

In order to obtain the distribution of v_w along x, the integration process described in appendix A is used. This procedure is briefly as follows: At $x + \Delta x$

$$Z_{x+\Delta x}^{(0)} = Z_x + \left(\frac{dZ}{dx}\right)_x \Delta x$$

The value of $R_{\theta_c}^{(0)}$ at $x + \Delta x$ is then found from equation (18). The value of $K_{x+\Delta x}^{(0)}$ is found by use of figure 1. The value of $k_{x+\Delta x}^{(0)}$ is found from $Z_{x+\Delta x}^{(0)}$ and $\left(\frac{dU}{dx}\right)_{x+\Delta x}$ by use of the definition

$$k = Z \frac{dU}{dx}$$

when $K^{(0)}_{x+\Delta x}$ and $k^{(0)}_{x+\Delta x}$ are known, $k_1{}^{(0)}_{x+\Delta x}$ is found from equation (4) and the functions $g(K)$ and $f(K)$. The value of $\left(\frac{dZ}{dx}\right)^{(0)}_{x+\Delta x}$ is now found from equations (A2) and (A3). The iteration process described in appendix A is then used to find the final value of all the quantities at $x + \Delta x$. The value of v_w at $x + \Delta x$ is found from the equation

$$f_1 = \frac{k_1}{\sqrt{Z}}$$

where

$$f_1 = -v_w\sqrt{R_c}$$

The procedure is repeated to find v_w at $x + 2\Delta x$ and so forth. When v_w becomes zero, the computation in the present examples is carried on with $k_1 = 0$.

The results of the computations for the NACA 64A010 airfoil are shown in figure 8. The behavior of the curves in figure 8(a) confirms the prediction of figure 6 that for $v_w = 0$ an increase in $\overline{\theta}$ increases K if $K > -1$. The distributions of v_w along x for $(v_w)_s = 0.0151$ and for $(v_w)_s = 0.0515$ are shown in figure 8(c) for the region where $v_w > 0$. The variation of R_θ and R_{θ_c} for $(v_w)_s = 0$, $(v_w)_s = 0.0151$, and $(v_w)_s = 0.0515$ is shown in figures 8(b), 8(d), and 8(e), respectively. In figure 8(f) is shown the distribution of R_{θ_c}/R_θ along x for the three distributions of v_w with x. The ratio of the boundary-layer thicknesses with blowing to those without blowing is shown in figure 8(g).

There are two main results of the computations for the NACA 64A010 airfoil section. The first is that except for the region between $x = 0.038$ and $x = 0.06$ (fig. 8(f)) the stability is decreased by the blowing; for $x > 0.06$ the decrease is small. The second result is that, although there is a large increase in boundary-layer thickness near the stagnation point (fig. 8(g)), the amount of the increase in

thickness decreases rapidly until at the pressure minimum the boundary-layer thickness for $(v_w)_s = 0.0151$ is only about 2 percent and the boundary-layer thickness for $(v_w)_s = 0.0515$ only about 5 percent greater than for $(v_w)_s = 0$. Thus, the only effect making transition less likely is the increased boundary-layer thickness and this increased thickness is present over only the foremost portion of the airfoil.

The results of the computations for the NACA 64_2A015 airfoil are shown in figure 9. The behavior of the curves in figure 9(a) confirms the prediction of figure 6. The variation of v_w along x for $(v_w)_s = 0.0111$ and for $(v_w)_s = 0.0380$ are shown in figure 9(c) for the region where $v_w > 0$. Figures 9(b), 9(d), and 9(e) contain the variation of R_θ and of R_{θ_c} with x for $(v_w)_s = 0$, $(v_w)_s = 0.0111$, and $(v_w)_s = 0.0380$, respectively. In figure 9(f) is shown the distribution of R_{θ_c}/R_θ along x for the three distributions of $(v_w)_s$ along x. Figure 9(g) contains the ratios of boundary-layer thicknesses with blowing to those without blowing. There are again two main results. For the NACA 64_2A015 airfoil the ratio R_{θ_c}/R_θ is greater for $(v_w)_s > 0$ than for $(v_w)_s = 0$ for values of x between about 0.065 and 0.30 (fig. 9(f)). The ratio of boundary-layer thickness with blowing to that without blowing (fig. 9(g)) shows the same behavior as for the NACA 64A010 airfoil.

The chosen distribution of blowing has thus shown a greater effect in reducing the likelihood of transition on the NACA 64_2A015 airfoil than on the NACA 64A010 airfoil. On the NACA 64_2A015 airfoil the chosen distribution of blowing has, in addition to the increase in boundary-layer thickness, also produced an increase in stability that is noticeable to about $x = 0.30$.

Power required for blowing.- The power required for blowing is

$$P = \frac{\overline{Q}\,\overline{\Delta H}}{E_B}$$

where $\overline{Q}$ is the volume of fluid blown out per second, $\overline{\Delta H}$ is the total pressure added to the fluid by a system within the aircraft, and E_B is the efficiency of the entire boundary-layer control system.

The quantity $\overline{Q}\,\overline{\Delta H}$ is obtained by integrating $\overline{v}_w\,\overline{\Delta H}$ around the entire airfoil surface; thus

$$\overline{Q}\,\overline{\Delta H} = \oint \overline{v}_w\,\overline{\Delta H}\,d\overline{x}$$

Expressed as a drag coefficient, the power required for boundary-layer control is:

$$C_{D_P} = \frac{PE_P}{\frac{\bar{\rho}_o}{2}\,\bar{U}_o^3\bar{c}} = \frac{E_P}{E_B}\oint \frac{\bar{v}_w}{\bar{U}_o}\,\frac{\overline{\Delta H}}{\bar{q}_o}\,d\,\frac{\bar{x}}{\bar{c}}$$

where E_P is the efficiency of the aircraft propulsive system. Then,

$$C_{D_P} = \frac{E_P}{E_B}\oint v_w\,\frac{\overline{\Delta H}}{\bar{q}_o}\,dx \tag{19}$$

If no fluid originates or is retained in the aircraft, the total drag coefficient is

$$C_{D_t} = 2\left(\frac{\bar{\theta}}{\bar{c}}\right)_\infty + \frac{E_P}{E_B}\oint v_w\,\frac{\overline{\Delta H}}{\bar{q}_o}\,dx$$

where $2\left(\frac{\bar{\theta}}{\bar{c}}\right)_\infty$ is the wake drag coefficient of the airfoil (reference 16).

The expression for C_{D_P} (equation (19)) can also be written as

$$C_{D_P} = \frac{E_P}{E_B}\left(\frac{\overline{\Delta H}}{\bar{q}_o}\right)_m \oint v_w\,dx \tag{20}$$

where $\left(\frac{\overline{\Delta H}}{\bar{q}_o}\right)_m$ is an average pressure loss defined by

$$\left(\frac{\overline{\Delta H}}{\overline{q}_o}\right)_m = \frac{\oint v_w\left(\frac{\overline{\Delta H}}{\overline{q}_o}\right)dx}{\oint v_w\ dx}$$

Now

$$\oint v_w\ dx = \frac{\oint \overline{v}_w\ d\overline{x}}{\overline{U}_o\overline{c}} = C_Q$$

Therefore

$$C_{D_P} = \frac{E_P}{E_B}\left(\frac{\overline{\Delta H}}{\overline{q}_o}\right)_m C_Q$$

The values of C_Q for the NACA 64A010 and NACA 64_2A015 airfoils are, for $\alpha = 0^\circ$ and $R_c = 10^7$,

Airfoil	$(v_w)_s$	C_Q
NACA 64A010	0.0151 .0515	0.00026 .00058
NACA 64_2A015	.0111 .0380	.00032 .00070

Because of the small values of C_Q, the drag coefficient C_{D_P} will be appreciable only when the factor $\frac{E_P}{E_B}\left(\frac{\overline{\Delta H}}{\overline{q}_o}\right)_m$ is a multiple of unity.

DISCUSSION

The present analysis uses two approximate methods, namely, Schlichting's method (reference 11) and Lin's approximate formula (reference 12). The tests of the Schlichting method in reference 11 and the test in appendix B for blowing near the stagnation point give no reason to doubt that the Schlichting method correctly predicts the response of the boundary layer to changes in the variables that affect its behavior, namely, pressure gradient, Reynolds number, blowing, and so forth. The accuracy of the prediction, however, is known to depend on the particular case (see reference 11).

Reference 17 investigated the approximate Lin formula and concluded that the predicted critical Reynolds numbers agree well with those predicted by more elaborate calculations. Although the Lin formula has good accuracy, the exact prediction of the critical Reynolds number of a velocity profile requires a precise knowledge of the first and second derivatives of the velocity profile $u = u(y)$. It therefore seems likely that the main uncertainty in the predictions of $R_{\theta c}/R_{\theta}$ by the combined Schlichting and Lin methods lies in the Schlichting method which assumes that all velocity profiles form the particular single-parameter family given by equation (A1), appendix A.

In spite of the inexactness of the methods of analysis the result that an increase in boundary-layer thickness can increase the stability of the laminar boundary layer under the proper conditions is believed valid. It therefore follows that thinning the boundary layer will not always increase the boundary-layer stability. The present analysis, however, does not predict the effects obtained by placing slots on a surface (references 7, 8, and 9) because this investigation treats the effect of a change in boundary-layer thickness alone and slots change not only the boundary-layer thickness but also, by their sink effect (reference 9), change the pressure distribution in their vicinity and, by introducing stagnation points, can produce convex velocity profiles on their downstream sides.

It is noted that the pressure drop along the surface required to make any thickening of the boundary layer result in an increase in stability is not very large. For example, the NACA 64_2A015 airfoil at $\alpha = 0^{\circ}$ has a large enough pressure drop over the forward $22\frac{1}{2}$ percent of the surface to make any increase in boundary-layer thickness increase the stability.

The result that the effective height of surface irregularities can be decreased by an increase in boundary-layer thickness without a decrease

in stability and the fact that the consistent attainment of laminar flow in flight is prevented by surface irregularities makes it important to find a method that can increase the boundary-layer thickness without itself causing transition.

In the present work an investigation was made of the feasibility of increasing boundary-layer thicknesses by blowing over the foremost portion of an airfoil. In order to make the effects clear, large blowing velocities at the stagnation point were chosen. In order for the Von Kármán momentum equation to be valid, however, it is necessary that v_w be of the order of $\frac{1}{\sqrt{R_c}}$ or that $U = \left(\frac{dU}{dx}\right)_s x$. That is, either the boundary-layer-theory assumptions must be satisfied or (see appendix C) the flow must be a stagnation-point flow. For definiteness, it is assumed that v_w must be less than $\frac{10}{\sqrt{R_c}}$; at $R_c = 10^7$, v_w must thus be less than 0.003 if $U \neq \left(\frac{dU}{dx}\right)_s x$.

For the NACA 64A010 airfoil $U = 174.7x$ to about $x = 0.003$ with less than 10-percent error; thus the stagnation-point flow extends to about $x = 0.003$. In this region large values of v_w do not invalidate the Von Kármán momentum equation; therefore the Schlichting method remains valid for large v_w for x less than about 0.003. For $(v_w)_s = 0.0151$ however, $v_w > 0.003$ for values of x between 0.003 and 0.011 (fig. 8(c)) and for $(v_w)_s = 0.0515$, $v_w > 0.003$ for values of x between 0.003 and 0.012 (fig. 8(c)). Therefore in the region lying roughly between $x = 0.003$ and $x = 0.012$ and about 0.01 in length, the values of v_w are large enough to introduce an additional uncertainty into the predictions of the calculations for the NACA 64A010 airfoil. A similar region exists between $x = 0.007$ and $x = 0.015$ for $(v_w)_s = 0.0111$ (fig. 9(c)) and between $x = 0.007$ and $x = 0.020$ for $(v_w)_s = 0.0380$ (fig. 9(c)) on the NACA 64_2A015 airfoil. The region in which the Schlichting method is probably invalid grows with an increase in $(v_w)_s$ so that it is inadvisable to make calculations for larger values of $(v_w)_s$ on the NACA 64A010 and NACA 64_2A015 airfoils at $\alpha = 0^\circ$ and $R_c = 10^7$.

Although the blowing velocities were so large that the boundary-layer assumptions were probably violated in a small area at the end of the stagnation-point-flow region, the boundary-layer thickness was increased significantly over only the foremost portion of the airfoils.

Whether larger blowing velocities can appreciably increase the boundary-layer thickness over larger portions of the surface than found in the present work must therefore be determined experimentally.

CONCLUDING REMARKS

In order to investigate the possibility that an increase in boundary-layer thickness could increase the local critical Reynolds number more than the local boundary-layer Reynolds number, computations have been made by combining the Schlichting method with the Lin method for the calculation of the critical Reynolds number of a velocity profile. The computations indicate that in a region of falling pressure on an impervious surface an increase in boundary-layer thickness can cause the velocity profile shape to be changed enough by the increase in effective pressure gradient so that the ratio of the local critical Reynolds number to the local boundary-layer Reynolds number is increased. It thus appears that the local stability of the boundary layer can be increased by a local increase in boundary-layer thickness. The computations also indicate that similar effects occur when there is flow through the surface; in this case the results depend on the effective flow through the surface as well as on the effective pressure gradient.

These calculations suggest that an increase in boundary-layer thickness can decrease the disturbing effect of roughness particles without a decrease in stability. This conclusion is implied by the result that an increase in boundary-layer thickness reduces the velocity at a fixed distance from the surface more than the change in velocity profile increases the velocity. One method of increasing the boundary-layer thickness, namely, blowing near the stagnation point, has been investigated theoretically and seems to have limited potentialities because the blowing produces a significant increase in boundary-layer thickness only over the foremost portion of the airfoil.

Langley Aeronautical Laboratory
National Advisory Committee for Aeronautics
Langley Field, Va., March 19, 1952

APPENDIX A

MODIFICATION OF THE SCHLICHTING METHOD

The Schlichting method assumes that all velocity profiles of the laminar boundary layer form the single-parameter family

$$\frac{u}{U} = F_1(\eta) + KF_2(\eta) \qquad ; \qquad \eta = \frac{\bar{y}}{\bar{\delta}_1(x)} \tag{A1}$$

where K is the velocity-profile shape parameter. The functions F_1 and F_2 are (see reference 11):

$$F_1 = 1 - e^{-\eta}$$

and

$$F_2 = F_1 - \sin\left(\frac{\pi}{6}\eta\right) \qquad (0 < \eta \leqq 3)$$

$$F_2 = -e^{-\eta} \qquad (\eta \geqq 3)$$

The function F_1 represents the asymptotic suction profile (reference 11) and the term $\sin\left(\frac{\pi}{6}\eta\right)$ represents an approximation to the Blasius profile for the flat plate ($K = -1$). With this relation for the velocity profile, Schlichting uses the momentum equation in the form

$$\frac{\bar{U}\bar{\theta}}{\bar{\nu}}\frac{d\bar{\theta}}{d\bar{x}} + \left(2 + \frac{\bar{\delta}^*}{\bar{\theta}}\right)\frac{\bar{\theta}^2}{\bar{\nu}}\frac{d\bar{U}}{d\bar{x}} - \frac{\bar{v}_w\bar{\theta}}{\bar{\nu}} = \frac{\bar{\tau}_w\bar{\theta}}{\bar{\mu}\bar{U}}$$

By introducing the substitutions

$$k = \frac{\overline{\theta}^2}{\overline{\nu}} \frac{d\overline{U}}{d\overline{x}} = Z \frac{dU}{dx}$$

$$k_1 = -\frac{\overline{v}_w \overline{\theta}}{\overline{\nu}} = f_1 \sqrt{Z}$$

and

$$f = \frac{\overline{\tau}_w \overline{\theta}}{\overline{\mu}\overline{U}}$$

where $Z = \theta^2 R_c$, the momentum equation can be written as

$$\frac{dZ}{dx} = \frac{G\left(k,k_1\right)}{U} \tag{A2}$$

where

$$G\left(k,k_1\right) = 2\left[f - k\left(2 + \frac{\delta^*}{\theta}\right) - k_1\right] \tag{A3}$$

The terms f and δ^*/θ are functions of the parameter K which is a function of k and k_1.

In order to compute the properties of the boundary layer, equation (A2) is integrated step by step to find $Z(x)$; therefore, $G(k,k_1)$ must be found at each step. Schlichting gives a plot of $G(k,k_1)$; the computation of $Z(x)$ therefore is made by using equation (A2), the definitions of k and k_1, and the plot of $G(k,k_1)$ (fig. 6 of reference 11). When any property of the shape of the velocity profiles is needed, the distribution of the shape parameter $K(x)$ must also be found. The parameter K, however, is given by Schlichting not as a function of k and k_1 but as a function of λ and λ_1; thus (equation (14) of reference 11)

$$K = \frac{\lambda + \lambda_1 - 1}{1 - \lambda_1\left(1 - \frac{\pi}{6}\right)} \tag{A4}$$

where

$$\lambda = \frac{\bar{\delta}_1^{\,2}}{\bar{\nu}} \frac{d\bar{U}}{d\bar{x}}$$

and

$$\lambda_1 = -\frac{\bar{v}_w \bar{\delta}_1}{\bar{\nu}}$$

In order to find $K(x)$, it is therefore first necessary to find $\lambda(x)$ and $\lambda_1(x)$ from $k(x)$ and $k_1(x)$, the quantities available from the computation of Z. The computed distributions $k(x)$ and $k_1(x)$ are converted to $\lambda(x)$ and $\lambda_1(x)$ by two sets of curves, one, values of λ against k for constant values of k_1, the other, values of λ_1 against k for constant values of k_1. The distribution of the shape parameter $K(x)$ is then found from a plot of equation (A4) (fig. 3 of reference 11).

In the present investigation, properties of the boundary layer on an airfoil with blowing $\left(v_w > 0\right)$ had to be calculated. Because the curves given in reference 11 for use in calculations are confined to $v_w \leqq 0$, it was necessary to extend them to $v_w > 0$. In doing this it was found that the curves of $\lambda(k,k_1)$ and $\lambda_1(k,k_1)$ could be eliminated and the extension of the Schlichting method to $v_w > 0$, simplified. The quantities λ and λ_1 then do not appear in a computation; K is found directly from k and k_1.

The quantities λ and λ_1 are eliminated by solving equation (22) of reference 11 for λ and equation (23) of reference 11 for λ_1 to obtain

$$\lambda = \frac{k}{g^2} \tag{A5}$$

and

$$\lambda_1 = \frac{k_1}{g} \tag{A6}$$

where $g = g(K) = \frac{\bar{\theta}}{\bar{\delta}_1}$. When equations (A5) and (A6) are used with equation (A4) the result is

$$g^2(K + 1) - g\left[1 + \left(1 - \frac{\pi}{6}\right)K\right]k_1 - k = 0 \tag{A7}$$

Equation (20) of reference 11, however, is

$$g\left[1 + \left(1 - \frac{\pi}{6}\right)K\right] = f(K)$$

Therefore, equation (A7) becomes:

$$g^2(K + 1) - fk_1 - k = 0 \tag{A8}$$

a relation between K, k, and k_1. The function $K(k,k_1)$, shown in figures 4(a) and 4(b), was calculated by fixing k_1 and calculating k for $-2.099 \leqq K \leqq 0$ from equation (A8). The functions $g(K)$ and $f(K)$ are given in reference 11.

The curves of $G(k,k_1)$ given by Schlichting (fig. 6 of reference 11) can thus be extended to negative values of k_1 (that is $v_w > 0$) by the use of equation (A3), figure 4, and the values of $f(K)$, $g(K)$, and $\delta^*/\theta(K)$ given in table 2 of reference 11. In the present work, however, because of the large range of k and k_1, it was more convenient to compute $G(k,k_1)$ at every step in x by using figures 4(a) and 4(b) and curves of $f(K)$, $g(K)$, and $\frac{\delta^*}{\theta}(K)$.

In order to integrate equation (A2), the value of Z at $x + \Delta x$ was found by the formula:

$$Z_{x+\Delta x}^{(0)} = Z_x + \left(\frac{dZ}{dx}\right)_x \Delta x$$

The value of $Z_{x+\Delta x}^{(0)}$ was used to find $\left(\frac{dZ}{dx}\right)_{x+\Delta x}^{(0)}$. A new value of $Z_{x+\Delta x}$ called $Z_{x+\Delta x}^{(1)}$ was then found from:

$$Z_{x+\Delta x}^{(1)} = Z_x + \frac{\Delta x}{2}\left[\left(\frac{dZ}{dx}\right)_x + \left(\frac{dZ}{dx}\right)_{x+\Delta x}^{(0)}\right]$$

This process was repeated either until there was no change between successive values of $\left(\frac{dZ}{dx}\right)_{x+\Delta x}$ or to $\left(\frac{dZ}{dx}\right)_{x+\Delta x}^{(2)}$. When $\left(\frac{dZ}{dx}\right)_{x+\Delta x}^{(2)}$ was not equal to $\left(\frac{dZ}{dx}\right)_{x+\Delta x}^{(1)}$ the step length was reduced. When $\left(\frac{dZ}{dx}\right)_{x+\Delta x}^{(2)}$ was equal to $\left(\frac{dZ}{dx}\right)_{x+\Delta x}^{(1)}$ the step length was not changed. When $\left(\frac{dZ}{dx}\right)_{x+\Delta x}^{(1)}$ was equal to $\left(\frac{dZ}{dx}\right)_{x+\Delta x}^{(0)}$ the step length was increased. In no case was a value of Δx larger than 0.05 used.

In order to begin a computation at the stagnation point, it is necessary to find the values of k and k_1 there. The requirement that $\frac{dZ}{dx}$ remain finite at the stagnation point ($U = 0$) means that $G(k,k_1) = 0$ (equation A2). The values of k and k_1 at the stagnation point therefore satisfy the equation

$$f - k\left(2 + \frac{\delta^*}{\theta}\right) - k_1 = 0 \tag{A9}$$

The variables f and δ^*/θ are functions of K only. Equation (A9) contains three variables, k, k_1, and K. In order to find another relation between k, k_1, and K, equation (A8) is used. There are then two equations in the two unknowns k and k_1:

$$f - k\left(2 + \frac{\delta^*}{\theta}\right) - k_1 = 0$$

and

$$g^2(K + 1) - k - fk_1 = 0$$

The solution is

$$k_s = \frac{f^2 - g^2(K + 1)}{\left(2 + \frac{\delta^*}{\theta}\right)f - 1} \tag{A10}$$

and

$$k_{1_s} = \frac{g^2(K + 1)\left(2 + \frac{\delta^*}{\theta}\right) - f}{\left(2 + \frac{\delta^*}{\theta}\right)f - 1} \tag{A11}$$

Equations (A10) and (A11) give the values of k and k_1 at the stagnation point as functions of K. Because K at the stagnation point is usually unknown, it is better to have k and k_1 as functions of known quantities. Schlichting (reference 11) introduces a quantity C_o defined as:

$$C_o = \left(\frac{k_1}{\sqrt{k}}\right)_s$$

By writing k_1 as

$$k_1 = -\frac{v_w}{U} R_\theta$$

and k as

$$k = \frac{R_\theta{}^2}{R_c}\left(\frac{1}{U^2}\frac{dU}{dx}\right)$$

the expression

$$C_o = \left(\frac{-v_w\sqrt{R_c}}{\sqrt{\frac{dU}{dx}}}\right)_s$$

is obtained. The quantities $(v_w)_s$, R_c, and $\left(\frac{dU}{dx}\right)_s$ are usually known. The connection between k_s, k_{1_s}, K_s, and C_o is shown in figure 12.

Although equation (A2) leads to

$$\frac{dZ}{dx} = \frac{0}{0}$$

at the stagnation point, an application of L'Hospital's Rule results in a definite expression for $\left(\frac{dZ}{dx}\right)_s$; it is

$$\left(\frac{dZ}{dx}\right)_s = \left[\frac{Z\frac{d^2U}{dx^2}\frac{\partial G}{\partial k} + \frac{df_1}{dx}\sqrt{Z}\frac{\partial G}{\partial k_1}}{\frac{dU}{dx}\left(1 - \frac{\partial G}{\partial k}\right) - \frac{f_1}{2\sqrt{Z}}\frac{\partial G}{\partial k_1}}\right]_s$$

For all computations in the present work $\left(\frac{dZ}{dx}\right)_s = 0$ because for a symmetrical airfoil at zero angle of attack $\left(\frac{d^2U}{dx^2}\right)_s = 0$ and because in the present work $\left(\frac{df_1}{dx}\right)_s = 0$.

APPENDIX B

FLOW AT THE STAGNATION POINT FOR LARGE BLOWING QUANTITIES

At the stagnation point the requirement that $\frac{dZ}{dx}$ remains finite although $U = 0$ means that $G(k,k_1) = 0$ at the stagnation point. The expression for $G(k,k_1)$ is

$$G(k,k_1) = 2\left[f - k\left(2 + \frac{\delta^*}{\theta}\right) - k_1\right] \tag{B1}$$

Therefore, at the stagnation point,

$$f - k\left(2 + \frac{\delta^*}{\theta}\right) - k_1 = 0 \tag{B2}$$

Now divide by k_1; the result is

$$\frac{f}{k_1} - \frac{k}{k_1}\left(2 + \frac{\delta^*}{\theta}\right) - 1 = 0 \tag{B3}$$

For the stagnation-point flow, k is positive. The maximum value that f can ever have is 0.5; the maximum value of $\frac{\delta^*}{\theta}$ is 4.64. Therefore, when k_1 becomes very large and negative, equation (B3) becomes

$$\frac{k}{k_1} = \frac{-1}{2 + \frac{\delta^*}{\theta}} \tag{B4}$$

The equation relating K, k, and k_1 also must apply; it is

$$g^2(K + 1) - k - fk_1 = 0 \tag{B5}$$

Now divide by k_1; the result is

$$\frac{g^2(K + 1)}{k_1} - \frac{k}{k_1} - f = 0 \tag{B6}$$

the maximum value of $g^2(K + 1)$ is 0.25; therefore, when k_1 becomes very large and negative, equation (B6) becomes

$$\frac{k}{k_1} = -f \tag{B7}$$

Therefore, for $G = 0$, k becomes large and positive as k_1 becomes large and negative. If equations (B4) and (B7) are combined, the result is

$$f\left(2 + \frac{\delta^*}{\theta}\right) - 1 = 0 \tag{B8}$$

Now (reference 11)

$$f = \left[1 + \left(1 - \frac{\pi}{6}\right)K\right]\left(c_o + c_1K + c_2K^2\right)$$

and (reference 11)

$$\frac{\delta^*}{\theta} = \frac{1 - \left(2 - \frac{6}{\pi}\right)K}{c_o + c_1K + c_2K^2}$$

Equation (B8) is then

$$\left[1 + \left(1 - \frac{\pi}{6}\right)K\right]\left[2\left(c_o + c_1K + c_2K^2\right) + 1 - \left(2 - \frac{6}{\pi}\right)K\right] - 1 = 0 \tag{B9}$$

By substituting the values (reference 11)

$$c_1 - c_2 = 2 - \frac{6}{\pi}$$

$$c_o = \frac{1}{2}$$

it can be shown by trial that $K = -1$ is a root of equation (B9). The other two roots are found to be

$$K = -4.95$$

and

$$K = 8.96$$

Because both are outside the permissible range of K $(-2.099 \leqq K \leqq 0)$, $K = -1$ is the only valid root of equation (B8). Therefore, for a stagnation-point flow with very large positive v_w the velocity profile becomes the Schlichting flat-plate profile

$$\frac{u}{U} = \sin\left(\frac{\pi}{6}\eta\right) \tag{B10}$$

The relation between K, k, and k_1 at the stagnation point for all values of k_1 is given by equations (A10) and (A11) and is shown in figures 4 and 12. By use of equations (A10) and (A11), it can be shown that $k \rightarrow 0$, $k_1 \rightarrow 0.5$, and $K \rightarrow 0$ as $C_o \rightarrow \infty$ and that $k \rightarrow \infty$, $k_1 \rightarrow -\infty$, and $K \rightarrow -1$ as $C_o \rightarrow -\infty$. From these results and figures 4 and 12 it is clear that for a stagnation-point flow $-1 \leqq K \leqq 0$. Therefore, the value of R_{θ_c} for a stagnation-point flow is always greater than 228 (see fig. 1) and the velocity profile never has an inflection point for $y > 0$; velocity profiles for $K \geqq -1$ have no inflection point for $y > 0$.

The velocity profile predicted by the Schlichting method for a stagnation-point flow with large positive v_w, namely, equation (B10) is now shown to be an exact solution of the Navier-Stokes equations. The work of reference 15 has shown that the exact solution of the Navier-Stokes equations for a stagnation-point flow with large positive v_w is

$$\frac{u}{U} = \sin\left(\frac{y}{v_w}\frac{dU}{dx}\right)$$

The variable η is

$$\eta = \frac{y}{\delta_1}$$

or

$$\eta = \left(\frac{y}{v_w}\frac{dU}{dx}\right)\left(\frac{\theta}{\delta_1}\right)\left(\frac{v_w}{\theta\frac{dU}{dx}}\right)$$

From the definitions of k and k_1 it follows that

$$\frac{k_1}{k} = -\frac{v_w}{\theta\frac{dU}{dx}}$$

In the limit for large v_w (large k_1), however, (see equation (B4))

$$\frac{k_1}{k} = -\left(2 + \frac{\delta^*}{\theta}\right)$$

Therefore

$$\eta = \left(\frac{y}{v_w}\frac{dU}{dx}\right)\left(\frac{\theta}{\delta_1}\right)\left(2 + \frac{\delta^*}{\theta}\right)$$

Now, from equation (17) of reference 11,

$$\frac{\theta}{\delta_1} = c_o + c_1K + c_2K^2$$

and from equation (19) of reference 11

$$\frac{\delta^*}{\theta} = \frac{1 - \left(2 - \frac{6}{\pi}\right)K}{c_o + c_1K + c_2K^2}$$

Therefore

$$\frac{\theta}{\delta_1}\left(2 + \frac{\delta^*}{\theta}\right) = 2\left(c_o + c_1K + c_2K^2\right) + 1 - \left(2 - \frac{6}{\pi}\right)K$$

In the limit as v_w gets large and positive, $K = -1$; therefore,

$$\frac{\theta}{\delta_1}\left(2 + \frac{\delta^*}{\theta}\right) = 2c_o - 2(c_1 - c_2) + 1 + \left(2 - \frac{6}{\pi}\right)$$

but, from reference 11,

$$c_o = \frac{1}{2}$$

and

$$c_1 - c_2 = 2 - \frac{6}{\pi}$$

Therefore,

$$\frac{\theta}{\delta_1}\left(2 + \frac{\delta^*}{\theta}\right) = 1 - 4 + 2\frac{6}{\pi} + 1 + 2 - \frac{6}{\pi} = \frac{6}{\pi}$$

and in the limit

$$\eta = \left(\frac{y}{v_w}\frac{dU}{dx}\right)\frac{6}{\pi}$$

Thus equation (B10) becomes

$$\frac{u}{U} = \sin\left(\frac{y}{v_w}\frac{dU}{dx}\right)$$

The Schlichting method therefore predicts the correct velocity profile for the stagnation-point flow for large blowing. Note, however, that the Schlichting method is incorrect in predicting that the velocity profile is the same as the flat-plate profile without blowing.

A comparison of the velocity profiles predicted by the approximate Schlichting method (reference 11) with some exact solutions of the boundary-layer equations for large v_w in a stagnation-point flow (reference 18) is shown in figure 13. The exact solutions of the boundary-layer equations for a stagnation-point flow are also solutions of the Navier-Stokes equations (reference 19, p. 82).

APPENDIX C

VON KÁRMÁN MOMENTUM EQUATION FOR STAGNATION-POINT FLOW

The stagnation-point flow, the flow in the region in which $U = \left(\frac{dU}{dx}\right)_s x$, can be described by the Navier-Stokes equations in nondimensional form; the equations are

$$u \frac{\partial u}{\partial x} + v \frac{\partial u}{\partial y} = - \frac{\partial p}{\partial x} + \frac{1}{R_c}\left(\frac{\partial^2 u}{\partial x^2} + \frac{\partial^2 u}{\partial y^2}\right) \tag{C1}$$

$$u \frac{\partial v}{\partial x} + v \frac{\partial v}{\partial y} = - \frac{\partial p}{\partial y} + \frac{1}{R_c}\left(\frac{\partial^2 v}{\partial x^2} + \frac{\partial^2 v}{\partial y^2}\right) \tag{C2}$$

The stream function for an inviscid stagnation-point flow with $v \neq 0$ at $y = 0$ is

$$\psi = axy - bx$$

(see reference 19 for the case $b = 0$) where

$$\psi = \frac{\bar{\psi}}{\bar{U}_o \bar{c}}$$

$$a = \frac{\bar{a}}{\bar{U}_o / \bar{c}}$$

and

$$b = \frac{\bar{b}}{\bar{U}_o}$$

The velocity components are $U = ax$ and $V = -ay + b$. By Bernoulli's theorem, the static pressure is

$$p = p_s - \frac{1}{2}\left(U^2 + v^2\right) = p_s - \frac{a^2}{2}\left[x^2 + y^2 - 2\left(\frac{b}{a}\right)y + \left(\frac{b}{a}\right)^2\right]$$

For a viscous fluid the expression for the stream function is generalized to

$$\psi = x\phi(y) - bx$$

and the expression for the static pressure, to

$$p = p_s - \frac{a^2}{2}\left[x^2 + F(y,b)\right] \tag{C3}$$

The velocity components are

$$\left.\begin{aligned} u &= \frac{\partial\psi}{\partial y} = x\frac{\partial\phi}{\partial y} \\ v &= -\frac{\partial\psi}{\partial x} = -\phi + b \end{aligned}\right\} \tag{C4}$$

The velocity components at $y = 0$ are $u = 0$ and $v = b$; at $y = \infty$ the x velocity component is the same as that for the inviscid fluid; that is

$$u = U = ax \tag{C5}$$

It will now be shown that the Von Kármán momentum equation results if equation (C1) is integrated with respect to y. From equations (C4) and the fact that the use of equations (C4) leads to a solution of the stagnation-point flow with blowing (references 15 and 18), it follows that

$$\frac{\partial^2 u}{\partial x^2} = 0$$

Equation (C1) thus becomes

$$u \frac{\partial u}{\partial x} + v \frac{\partial u}{\partial y} = - \frac{\partial p}{\partial x} + \frac{1}{R_c} \frac{\partial^2 u}{\partial y^2} \tag{C6}$$

Now integrate equation (C6) with respect to y; thus,

$$\int_0^l u \frac{\partial u}{\partial x} dy + \int_0^l v \frac{\partial u}{\partial y} dy = - \int_0^l \frac{\partial p}{\partial x} dy + \frac{1}{R_c} \int_0^l \frac{\partial^2 u}{\partial y^2} dy \tag{C7}$$

where l is a constant such that, for $y \geqq l$, $u = U = ax$.

By integration by parts it follows that

$$\int_0^l v \frac{\partial u}{\partial y} dy = vu\Big]_0^l - \int_0^l u \frac{\partial v}{\partial y} dy$$

But

$$v = \int_0^y \frac{\partial v}{\partial y} dy + v_w$$

and, by continuity,

$$\frac{\partial v}{\partial y} = - \frac{\partial u}{\partial x}$$

therefore,

$$\int_0^l v \frac{\partial u}{\partial y} dy = -U \int_0^l \frac{\partial u}{\partial x} dy + Uv_w + \int_0^l u \frac{\partial u}{\partial x} dy$$

Equation (C7) becomes

$$\int_0^l \frac{\partial u^2}{\partial x} dy - U \int_0^l \frac{\partial u}{\partial x} dy + Uv_w = - \int_0^l \frac{\partial p}{\partial x} dy + \frac{1}{R_c} \frac{\partial u}{\partial y}\Big]_0^l \tag{C8}$$

From equation (C3), $\frac{\partial p}{\partial x} = -a^2x$; $\frac{\partial p}{\partial x}$ is thus independent of y. By use of $U = ax$, $\frac{\partial p}{\partial x}$ can also be written as

$$\frac{\partial p}{\partial x} = -U \frac{dU}{dx} \tag{C9}$$

Equation (C8), after equation (C9) has been substituted and $\int_0^l \frac{\partial uU}{\partial x} dy$ added and subtracted, is

$$\int_0^l \frac{\partial u^2}{\partial x} dy - \int_0^l \frac{\partial uU}{\partial x} dy + \int_0^l \frac{\partial uU}{\partial x} dy -$$

$$U \int_0^l \frac{\partial u}{\partial x} dy - U \frac{dU}{dx} \int_0^l dy + Uv_w = - \frac{1}{R_c}\left(\frac{\partial u}{\partial y}\right)_s \tag{C10}$$

where $\frac{\partial u}{\partial y} = 0$ for $y \geq l$. After collecting terms and using

$$\frac{1}{R_c}\left(\frac{\partial u}{\partial y}\right)_w = \frac{\overline{\tau}_w}{\overline{\rho}_o \overline{U}_o{}^2}$$

equation (C10) becomes

$$\frac{d}{dx}\left[U^2 \int_0^l \frac{u}{U}\left(1 - \frac{u}{U}\right)dy\right] + U \frac{dU}{dx} \int_0^l \left(1 - \frac{u}{U}\right)dy - v_wU = \frac{\overline{\tau}_w}{\overline{\rho}_o \overline{U}_o{}^2}$$

But

$$\int_0^l \frac{u}{U}\left(1 - \frac{u}{U}\right)dy = \theta$$

and

$$\int_0^l \left(1 - \frac{u}{U}\right) dy = \delta^*$$

therefore, the result is the Von Kármán momentum equation

$$\frac{d\theta}{dx} + \frac{\theta}{U}\frac{dU}{dx}\left(2 + \frac{\delta^*}{\theta}\right) - \frac{v_w}{U} = \frac{\bar{\tau}_w}{\bar{\rho}_o \bar{U}^2}$$

Near the stagnation point $\left(\text{where } U = \left(\frac{dU}{dx}\right)_s x\right)$ the Von Kármán momentum equation is therefore obtainable directly from the Navier-Stokes equations of motion and is thus valid there even for large v_w. The Schlichting method is therefore not invalidated by the presence of large v_w in a stagnation-point flow.

REFERENCES

1. Abbott, Ira H., Von Doenhoff, Albert E., and Stivers, Louis S., Jr.: Summary of Airfoil Data. NACA Rep. 824, 1945. (Supersedes NACA ACR L5C05.)

2. Jacobs, Eastman N.: Preliminary Report on Laminar-Flow Airfoils and New Methods Adopted for Airfoil and Boundary-Layer Investigations. NACA ACR, June 1939.

3. Jones, B. Melvill: Flight Experiments on the Boundary Layer. Jour. Aero. Sci., vol. 5, no. 3, Jan. 1938, pp. 81-94.

4. Schlichting, H., and Ulrich, A.: Zur Berechnung des Umschlages laminar/turbulent. Bericht S10 der Lilienthal-Gesellschaft für Luftfahrtforschung, Preisausschreiben 1940, pp. 75-133.

5. Bussmann, K., and Munz, H.: De Stabilität der laminaren Reibungsschicht mit Absaugung. Jahrb. 1942 der deutschen Luftfahrtforschung, R. Oldenbourg (Munich), pp. I 36 - I 39.

6. Braslow, Albert L., Burrows, Dale L., Tetervin, Neal, and Visconti, Fioravante: Experimental and Theoretical Studies of Area Suction for the Control of the Laminar Boundary Layer on an NACA 64A010 Airfoil. NACA Rep. 1025, 1951. (Supersedes NACA TN 1905 by Burrows, Braslow, and Tetervin and NACA TN 2112 by Braslow and Visconti.)

7. Zalovcik, John A., Wetmore, J. W., and Von Doenhoff, Albert E.: Flight Investigation of Boundary-Layer Control by Suction Slots on an NACA 35-215 Low-Drag Airfoil At High Reynolds Numbers. NACA ACR 4B29, 1944.

8. Burrows, Dale L., and Schwartzberg, Milton A.: Experimental Investigation of an NACA 64A010 Airfoil Section with 41 Suction Slots on Each Surface for Control of Laminar Boundary Layer. NACA TN 2644, 1952.

9. Pfenninger, Werner: Investigations on Reductions of Friction on Wings, In Particular by Means of Boundary-Layer Suction. NACA TM 1181, 1947.

10. Loftin, Laurence, K., Jr.: Effects of Specific Types of Surface Roughness on Boundary-Layer Transition. NACA ACR L5J29a, 1946.

11. Schlichting, H.: An Approximate Method for Calculation of the Laminar Boundary Layer with Suction for Bodies of Arbitrary Shape. NACA TM 1216, 1949.

12. Lin, C. C.: On the Stability of Two-Dimensional Parallel Flows. Part I. Quarterly Appl. Math., vol. III, no. 2, July 1945, pp. 117-142; Part II, vol. III, no. 3, Oct. 1945, pp. 218-234; and Part III, vol. III, no. 4, Jan. 1946, pp. 277-301.

13. Pretsch, J: Die Stabilität einer ebenen Laminarströmung bei Druckgefälle und Druckanstieg. Jahrb. 1941 der deutschen Luftfahrtforschung, R. Oldenbourg (Munich), pp. I 158 - I 175.

14. Loftin, Laurence K., Jr.: Theoretical and Experimental Data for a Number of NACA 6A-Series Airfoil Sections. NACA Rep. 903, 1948. (Supersedes NACA TN 1368.)

15. Pretsch, J: Die laminare Grenzschicht bei starkem Absaugen und Ausblasen. Bericht B 44/F/02, Aerodynamische Versuchsanstalt Göttingen, Mar. 10, 1944.

16. Squire, H. B., and Young, A. D.: The Calculation of the Profile Drag of Aerofoils. R. & M. No. 1838, British A.R.C., 1938.

17. Chiarulli, P., and Freeman, J. C.: Stability of the Boundary Layer. Tech. Rep. No. F-TR-1197-IA, Air Materiel Command, U. S. Air Force, Aug. 1948.

18. Schlichting, H., and Bussmann, K.: Exakte Lösungen für die laminare Grenzschicht mit Absaugung und Ausblasen. Bericht 42/10, Aerodynamisches Institut der T. H. Braunschweig, July 29, 1942.

19. Schlichting, H.: Lecture Series "Boundary Layer Theory." Part I - Laminar Flows. NACA TM 1217, 1949.

TABLE I.- SUPPLEMENTARY INFORMATION FOR CURVES OF FIGURES 2 AND 5

(a) Values of J and related information

Curve	Value of J	Range of k_1	Range of K	Sign of root in equation (6)
Figures 2(a) and 5(a), $v_w > 0$				
1	10^4	$-10^4 \leqq k_1 \leqq -38$	$-2.068 \leqq K \leqq 0$	+
2	10	$-10.48 \leqq k_1 \leqq -1.071$	$-1.461 \leqq K \leqq 0$	+
3	1	$-1.366 \leqq k_1 \leqq -0.1869$	$-1.111 \leqq K \leqq 0$	+
4	.1	$-0.2791 \leqq k_1 \leqq -0.02113$	$-1.013 \leqq K \leqq 0$	+
5	.001	$-0.02287 \leqq k_1 \leqq -0.0002145$	$-1.00013 \leqq K \leqq 0$	+
6	-.001	$-0.0122 \leqq k_1 \leqq 0$	$-1.924 \leqq K \leqq -1$	-
7	-.1	$-0.1207 \leqq k_1 \leqq 0$	$-2.018 \leqq K \leqq -1$	-
8	-1	$-0.38 \leqq k_1 \leqq 0$	$-2.099 \leqq K \leqq -1$	-
9	-10	$-1.20 \leqq k_1 \leqq 0$	$-2.099 \leqq K \leqq -1$	-
10	-10^4	$-38 \leqq k_1 \leqq 0$	$-2.099 \leqq K \leqq -1$	-
11	10^4	$-38 \leqq k_1 \leqq 0$	$-2.068 \leqq K \leqq -1$	-
12	10	$-1.071 \leqq k_1 \leqq 0$	$-1.461 \leqq K \leqq -1$	
13	1	$-0.1869 \leqq k_1 \leqq 0$	$-1.111 \leqq K \leqq -1$	-
Figures 2(b) and 5(b), $v_w < 0$				
1	0.001	$0 \leqq k_1 \leqq 0.02187$	$-1 \leqq K \leqq 0$	-
2	.1	$0 \leqq k_1 \leqq 0.1791$	$-1 \leqq K \leqq 0$	-
3	1	$0 \leqq k_1 \leqq 0.3661$	$-1 \leqq K \leqq 0$	-
4	10	$0 \leqq k_1 \leqq 0.4770$	$-1 \leqq K \leqq 0$	-
5	10^4	$0 \leqq k_1 \leqq 0.5000$	$-1 \leqq K \leqq 0$	-
6	-10^4	$0 \leqq k_1 \leqq 0.5000$	$-1 \leqq K \leqq 0$	-
7	-10	$0 \leqq k_1 \leqq 0.5280$	$-1 \leqq K \leqq 0$	-
8	-1	$0 \leqq k_1 \leqq 0.2639$	$-1 \leqq K \leqq -0.8120$	-
9	-1	$0.2639 \leqq k_1 \leqq 0.4652$	$-1.346 \leqq K \leqq -0.8120$	+
10	-.1	$0.0218 \leqq k_1 \leqq 0.1277$	$-1.785 \leqq K \leqq -0.9859$	+
11	-.001	$0.0002147 \leqq k_1 \leqq 0.0123$	$-1.926 \leqq K \leqq -0.9999$	+

TABLE I.- SUPPLEMENTARY INFORMATION FOR CURVES OF FIGURES 2 AND 5 - Concluded

(b) Information for extreme values of K

Curve	K	k_1	$\frac{1}{\frac{v_w}{U}}\frac{R_{\theta c}}{R_\theta} \times 10^{-3}$	Condition limiting K (a)
Figures 2(a) and 5(a), $v_w > 0$				
1	0 -2.068	-10^4 -38	0.002 0	--- A
2	0 -1.461	-10.48 -1.071	1.909 .0356	--- A
3	0 -1.111	-1.366 -.1869	14.6 .700	--- A
4	0 -1.013	-.2791 -.02113	71.60 10.2	--- A
5	0 -1.00013	-.02287 -.0002145	875 1,063	--- A
6	-1 -1.924	0 -.0122	∞ .246	--- B
7	-1 -2.018	0 -.1207	∞ .0075	--- B
8	-1 -2.099	0 -.38	∞ 0	--- ---
9	-1 -2.099	0 -1.20	∞ 0	--- ---
10	-1 -2.099	0 -38	∞ 0	--- ---
11	-1 -2.068	0 -38	∞ 0	--- A
12	-1 -1.461	0 -1.071	∞ .0356	--- A
13	-1 -1.111	0 -.1869	∞ .700	--- A
Figures 2(b) and 5(b), $v_w < 0$				
1	0 -1	0.02187 0	-914.5 ∞	--- ---
2	0 -1	.1791 0	-111.7 ∞	--- ---
3	0 -1	.3661 0	-54.63 ∞	--- ---
4	0 -1	.4770 0	-41.93 ∞	--- ---
5	0 -1	.5000 0	-40.000 ∞	--- ---
6	0 -1	.5000 0	-40.000 ∞	--- ---
7	0 -1	.5280 0	-37.88 ∞	--- ---
8	-.8120 -1	.2639 0	-3.20 ∞	A ---
9	-.8120 -1.346	.2639 .4652	-3.20 -.120	A B
10	-.9859 -1.785	.0218 .1277	-11.5 -.0767	A B
11	-.9999 -1.926	.0002147 .0123	-1.080 -.102	A B

[a]Condition A: $1 + \frac{2g^2(K + 1)}{f^2 J} = 0$; condition B: $k_1 = \frac{\frac{dg^2(K + 1)}{dK}}{df/dK}$.

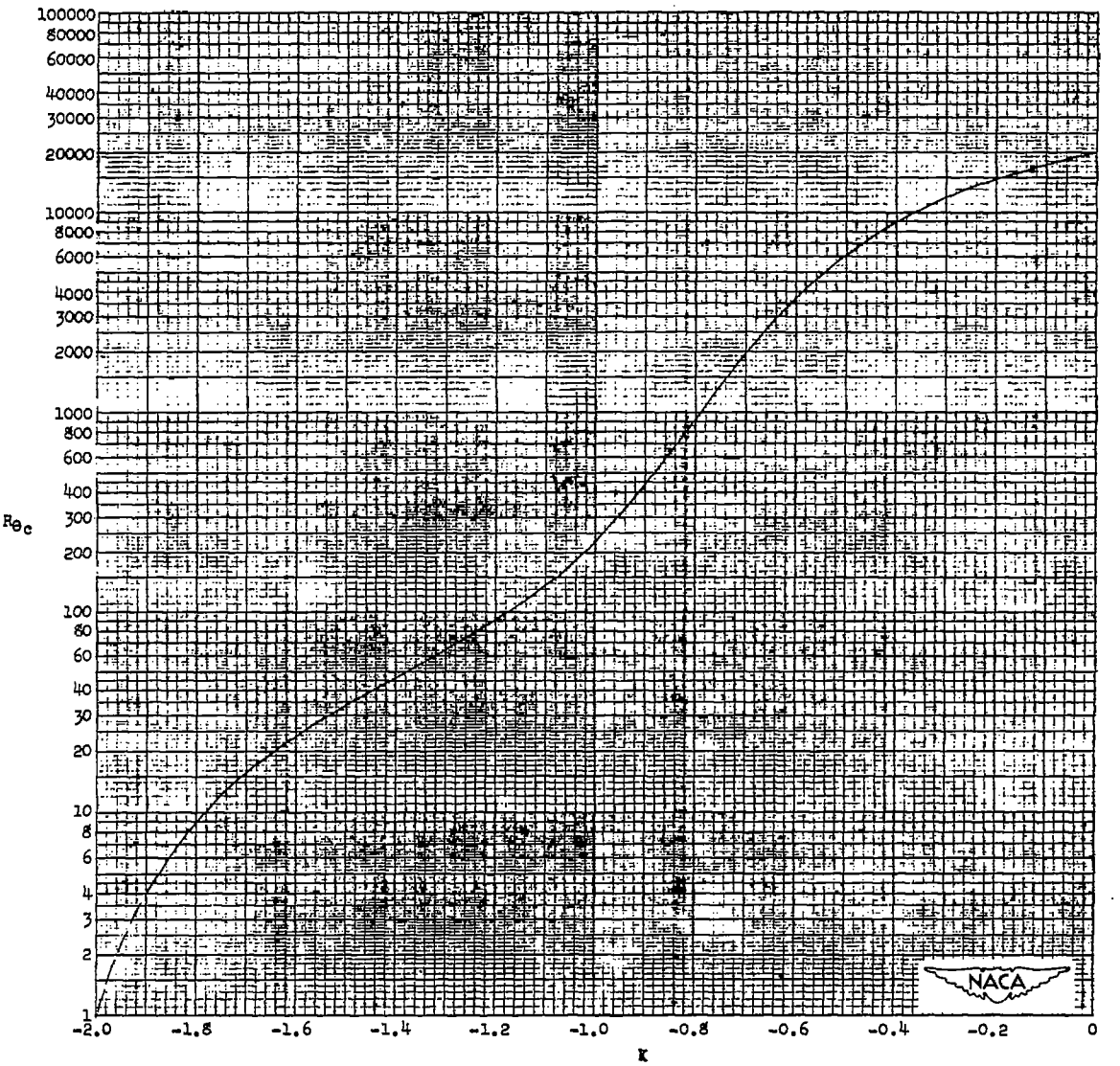

Figure 1.- Variation of critical boundary-layer Reynolds number R_{θ_c} with velocity-profile shape parameter K.

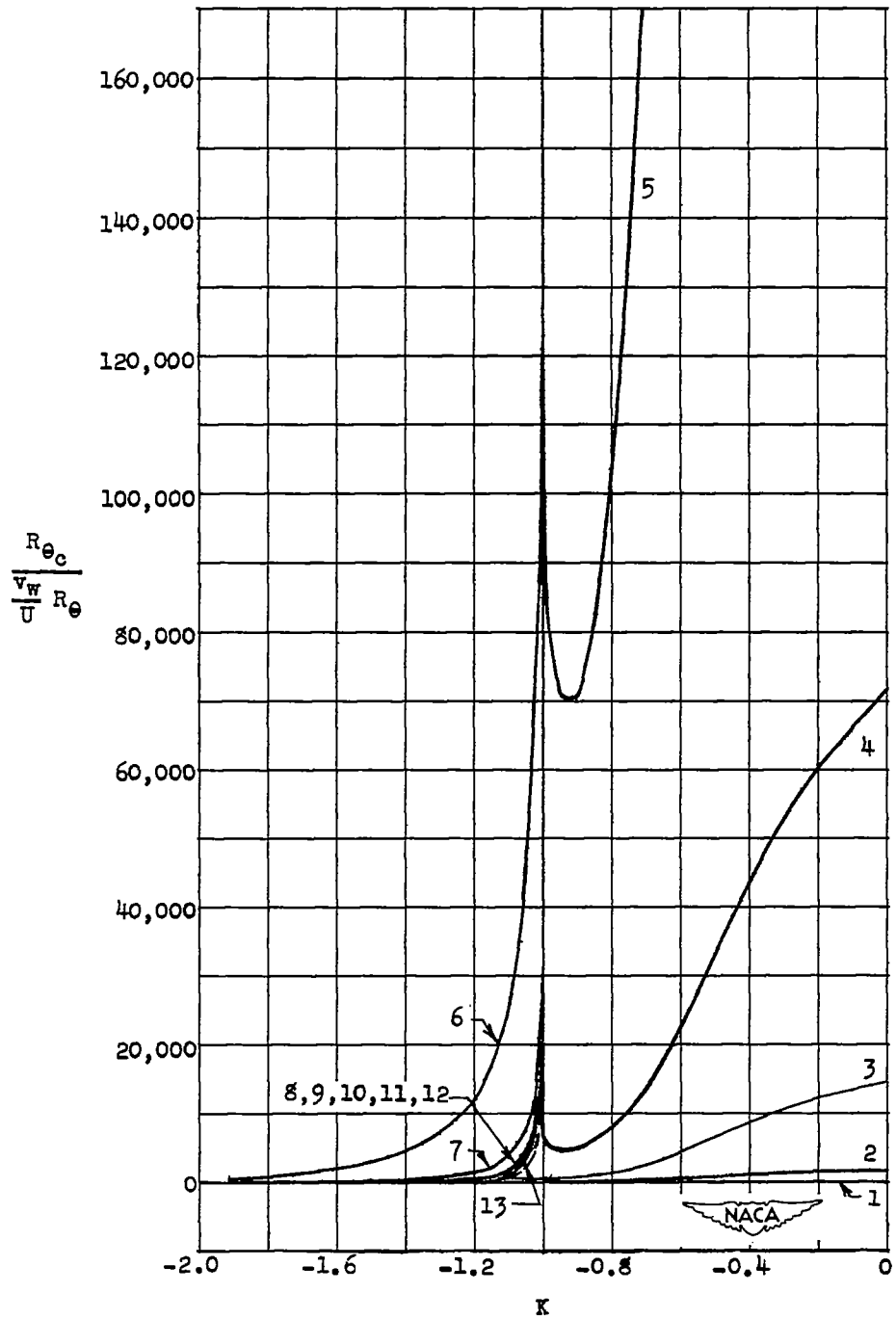

(a) $v_w > 0$.

Figure 2.- Variation of boundary-layer-stability parameter $\frac{R_{\theta_c}}{\frac{v_w}{U} R_\theta}$ with velocity-profile shape parameter K for fixed values of boundary-layer-control parameter J (see table I for values of J). The dashed line is the limiting curve (see equation (9)).

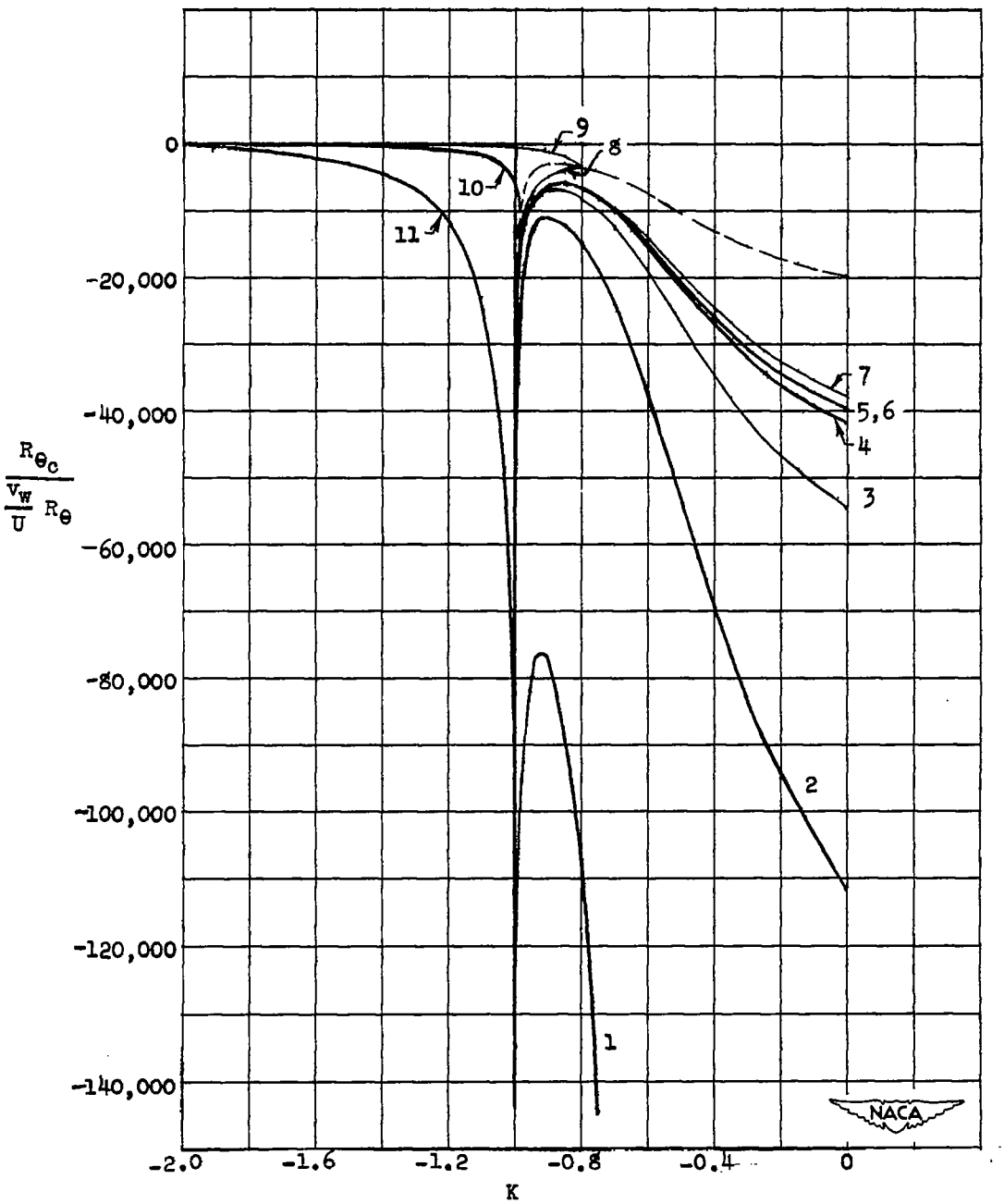

(b) $v_W < 0$.

Figure 2.- Concluded.

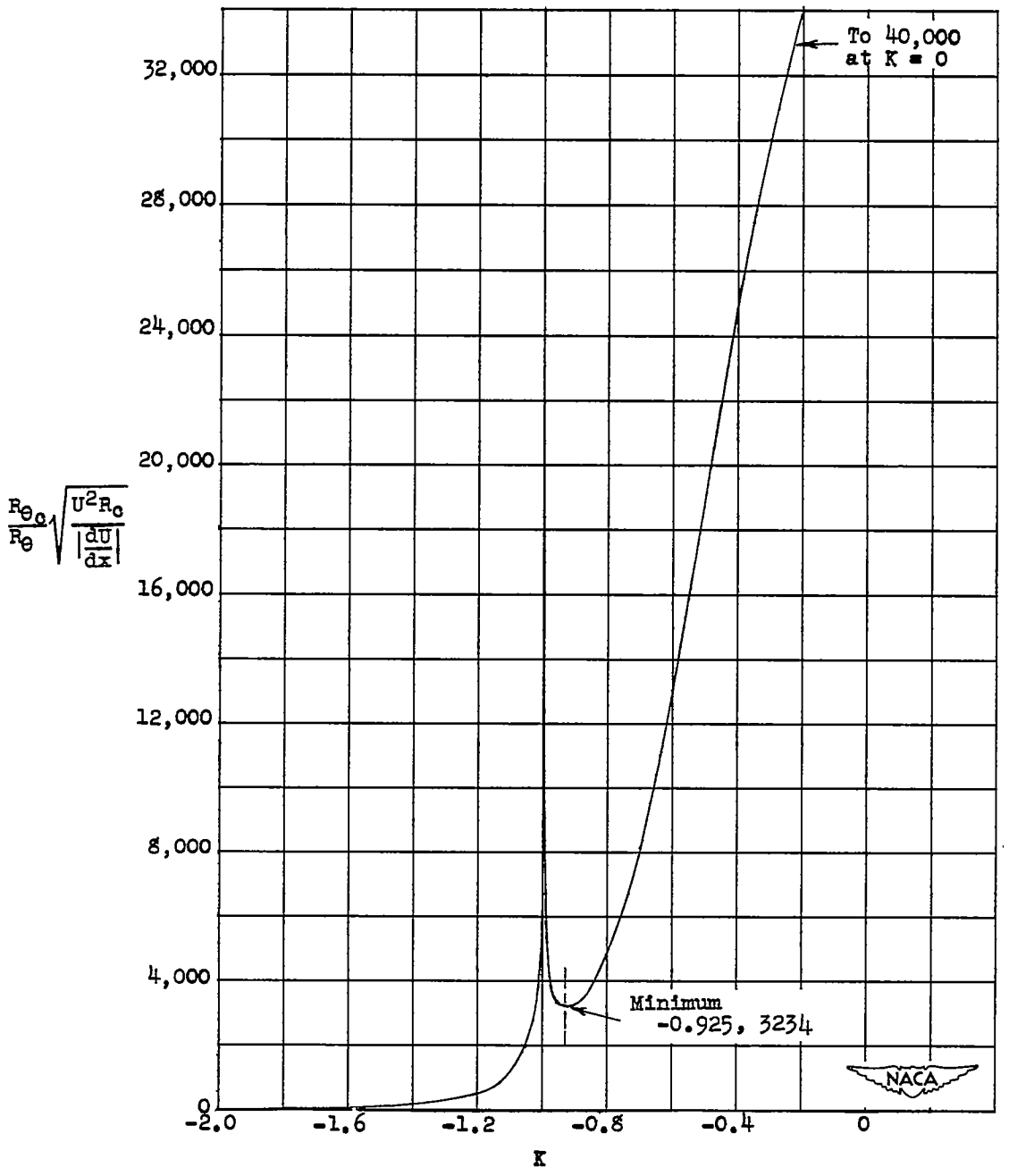

Figure 3.- Variation of $\frac{R_{\theta_c}}{R_\theta}\sqrt{\frac{U^2R_c}{\left|\frac{dU}{dx}\right|}}$, boundary-layer-stability parameter for no flow through the surface ($v_w = 0$), with velocity-profile shape parameter K.

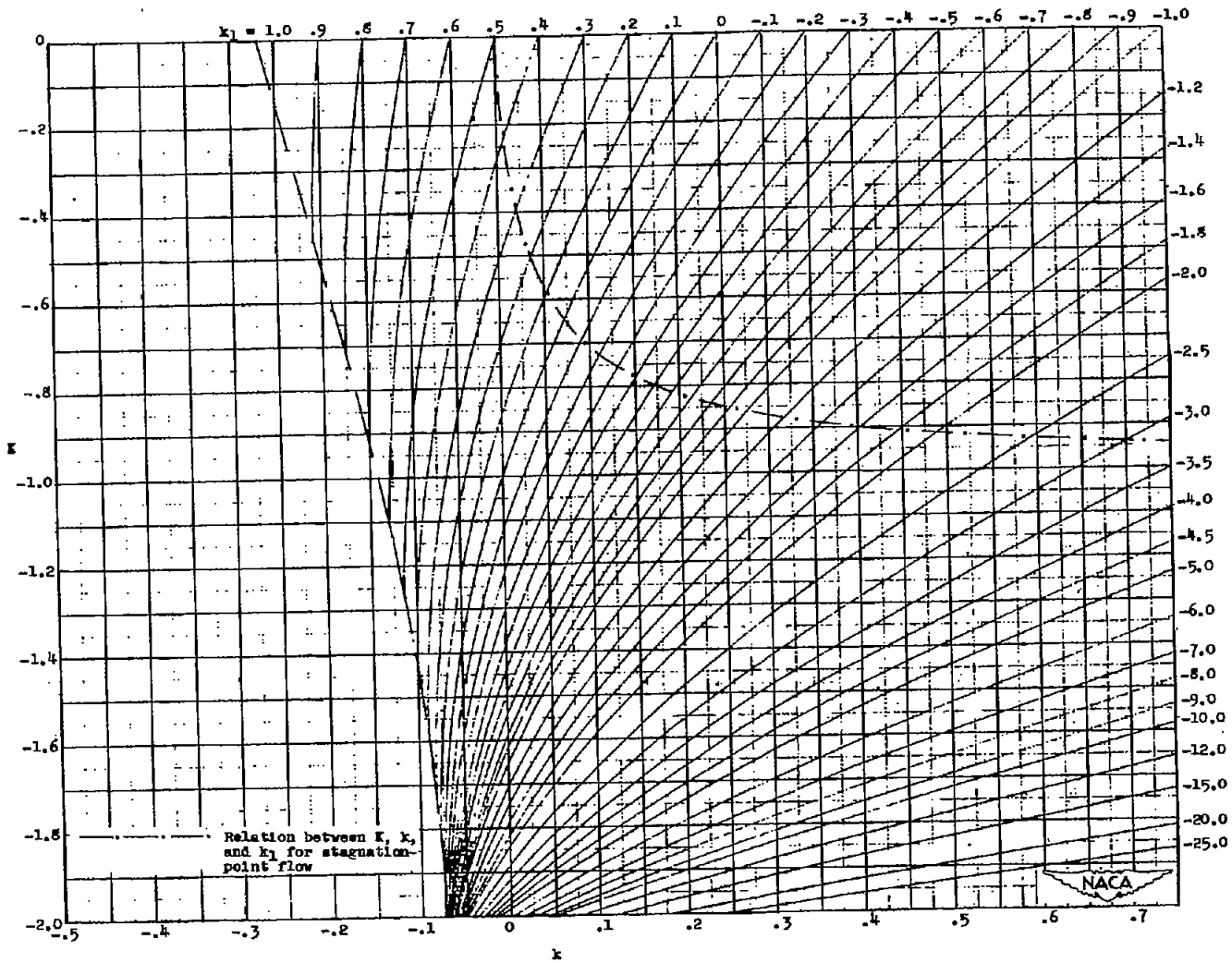

(a) $-0.2694 \leqq k \leqq 0.75$.

Figure 4.- Velocity-profile shape parameter K as a function of pressure-gradient parameter k and parameter of flow through surface k_1.

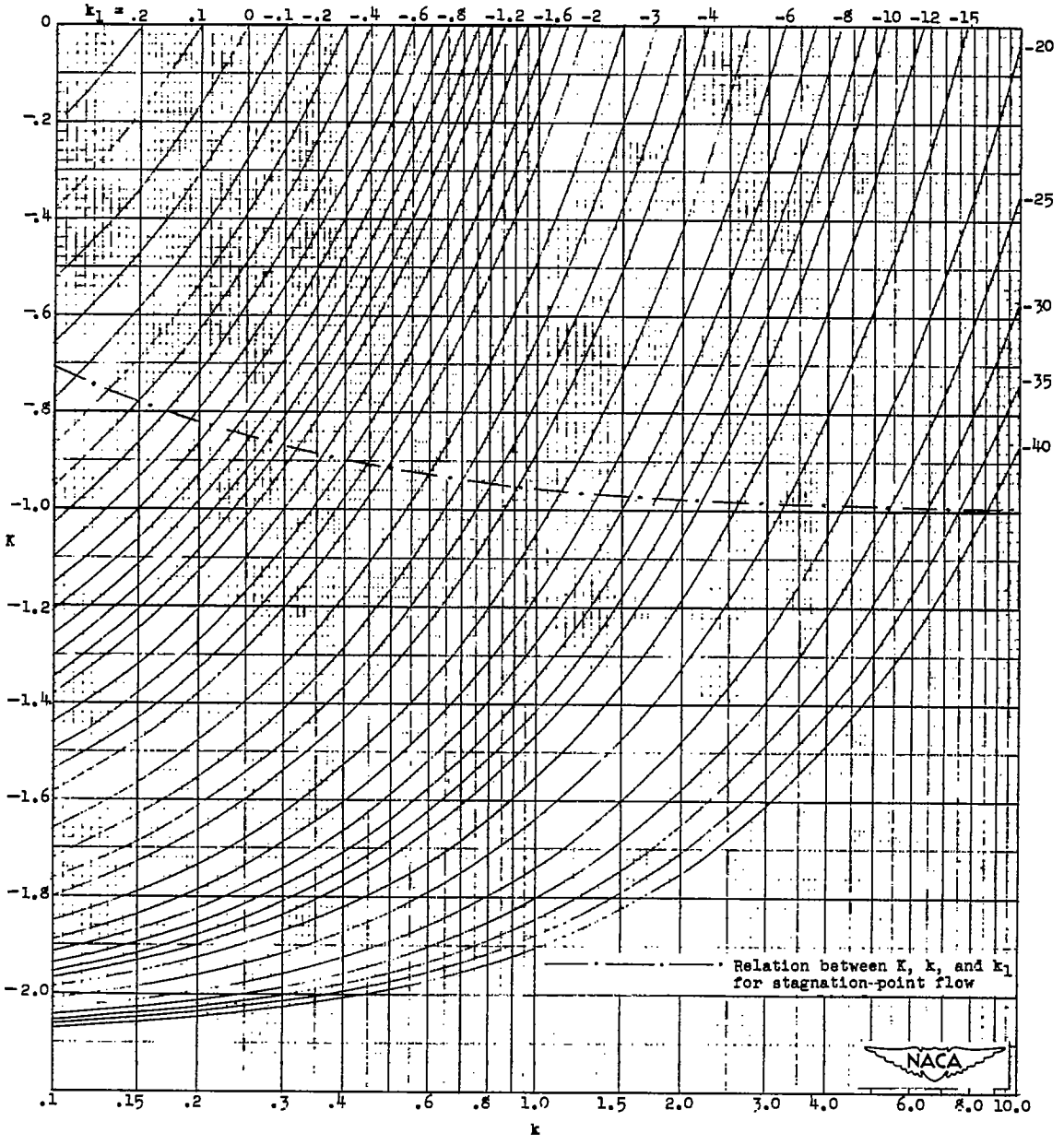

(b) $0.1 \leqq k \leqq 10.$

Figure 4.- Concluded.

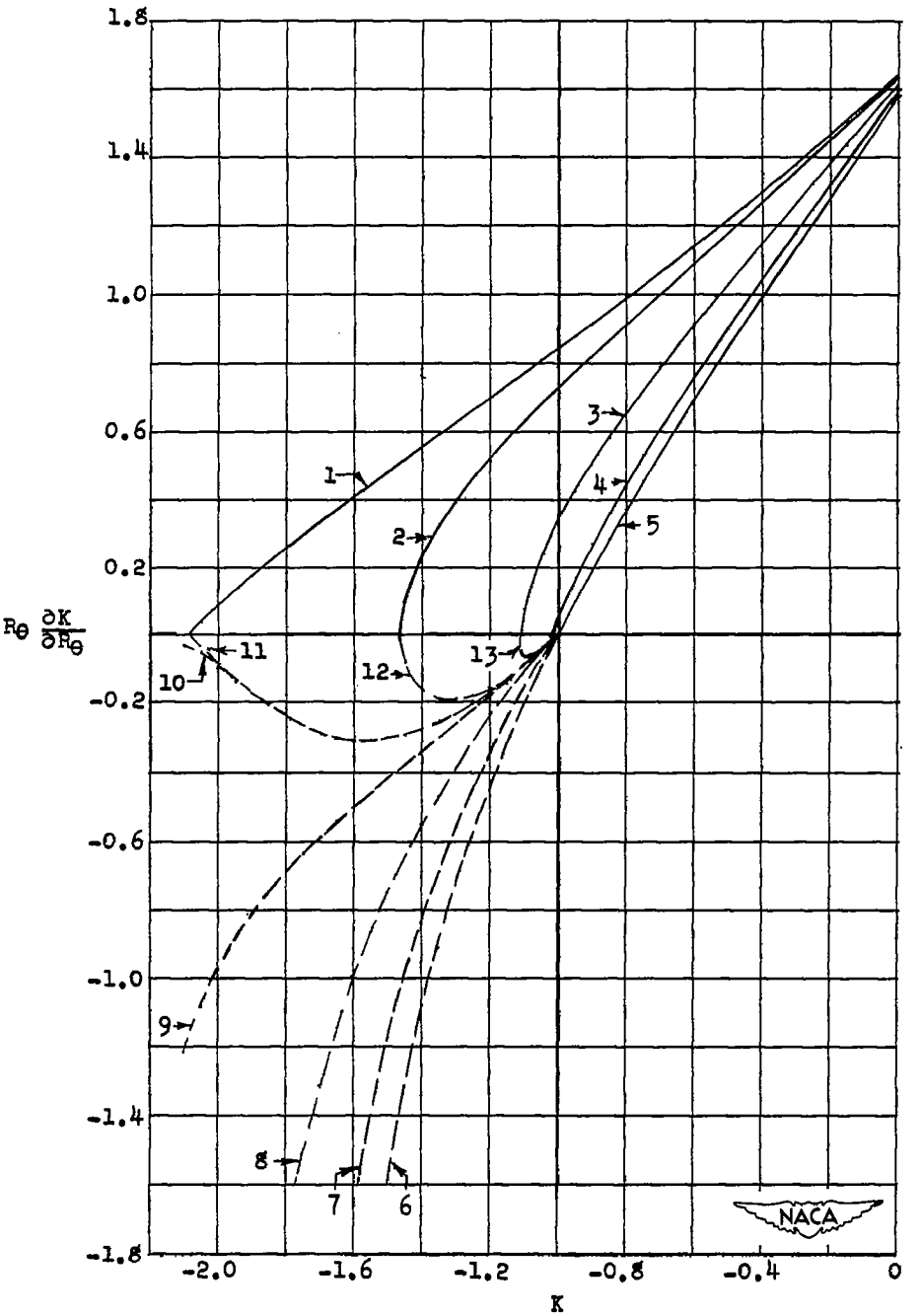

(a) $v_w > 0$.

Figure 5.- Variation with velocity-profile shape parameter K of $R_\theta \frac{\partial K}{\partial R_\theta}$, parameter of rate of change of K with boundary-layer thickness, for fixed values of boundary-layer-control parameter J (see table I for values of J).

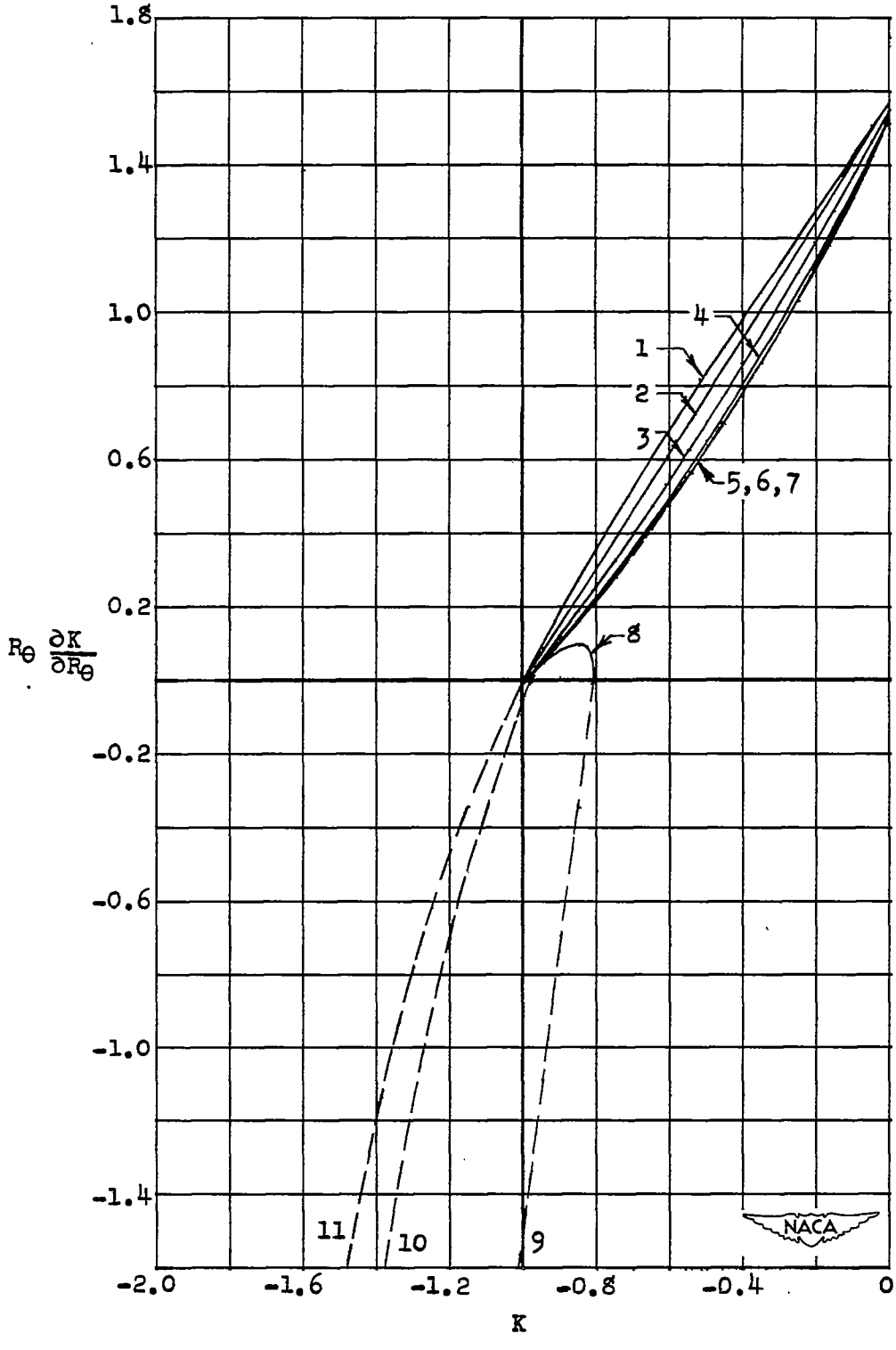

(b) $v_W < 0$.

Figure 5.- Concluded.

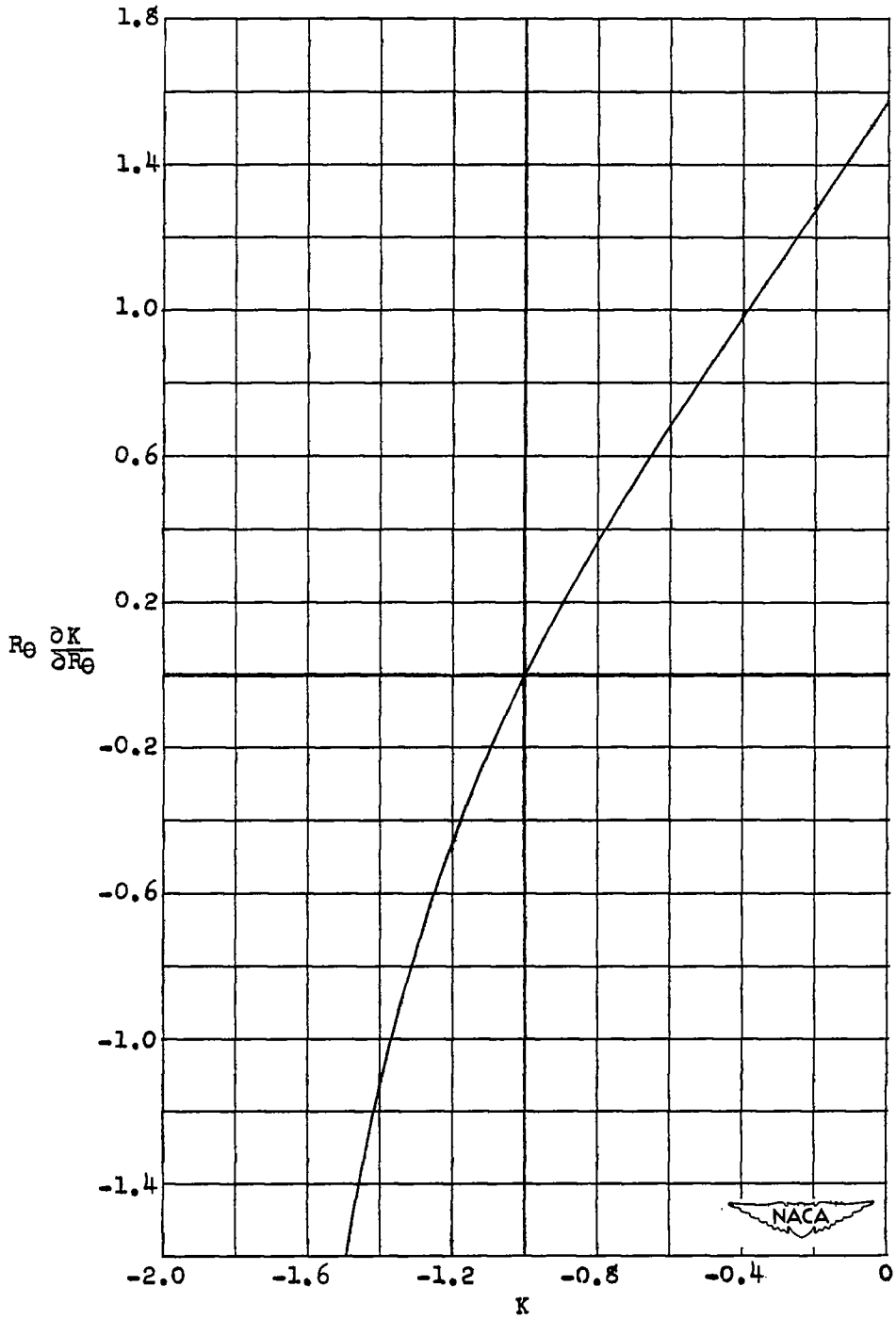

Figure 6.- Variation with velocity-profile shape parameter K of $R_\theta \frac{\partial K}{\partial R_\theta}$, parameter of rate of change of K with boundary-layer thickness, for no flow through surface ($v_w = 0$).

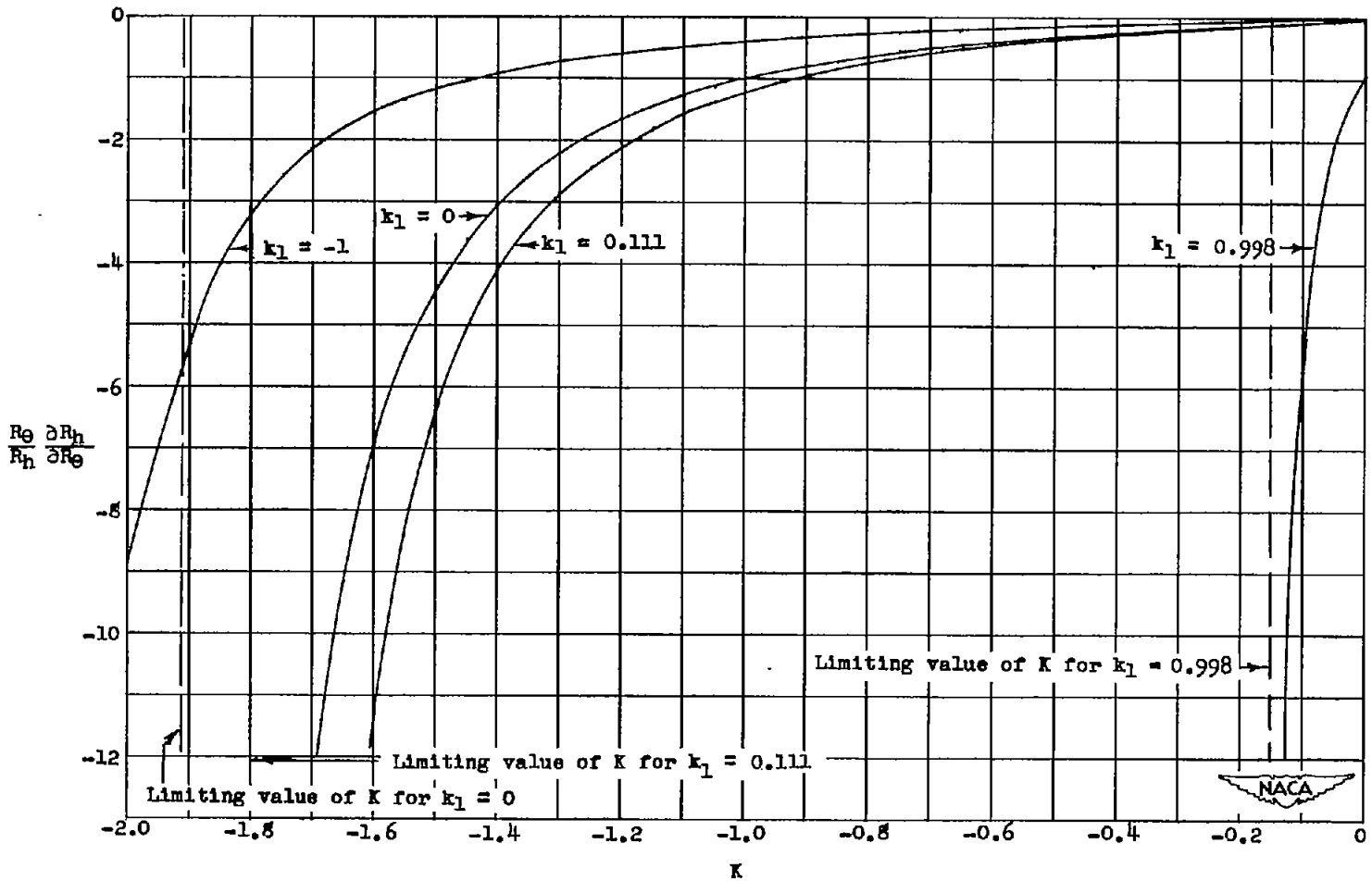

Figure 7.- Variation with velocity-profile shape parameter K of $\frac{R_\theta}{R_h}\frac{\partial R_h}{\partial R_\theta}$, parameter of rate of change of roughness Reynolds number R_h with boundary-layer thickness, for fixed values of parameter of flow through surface k_1.

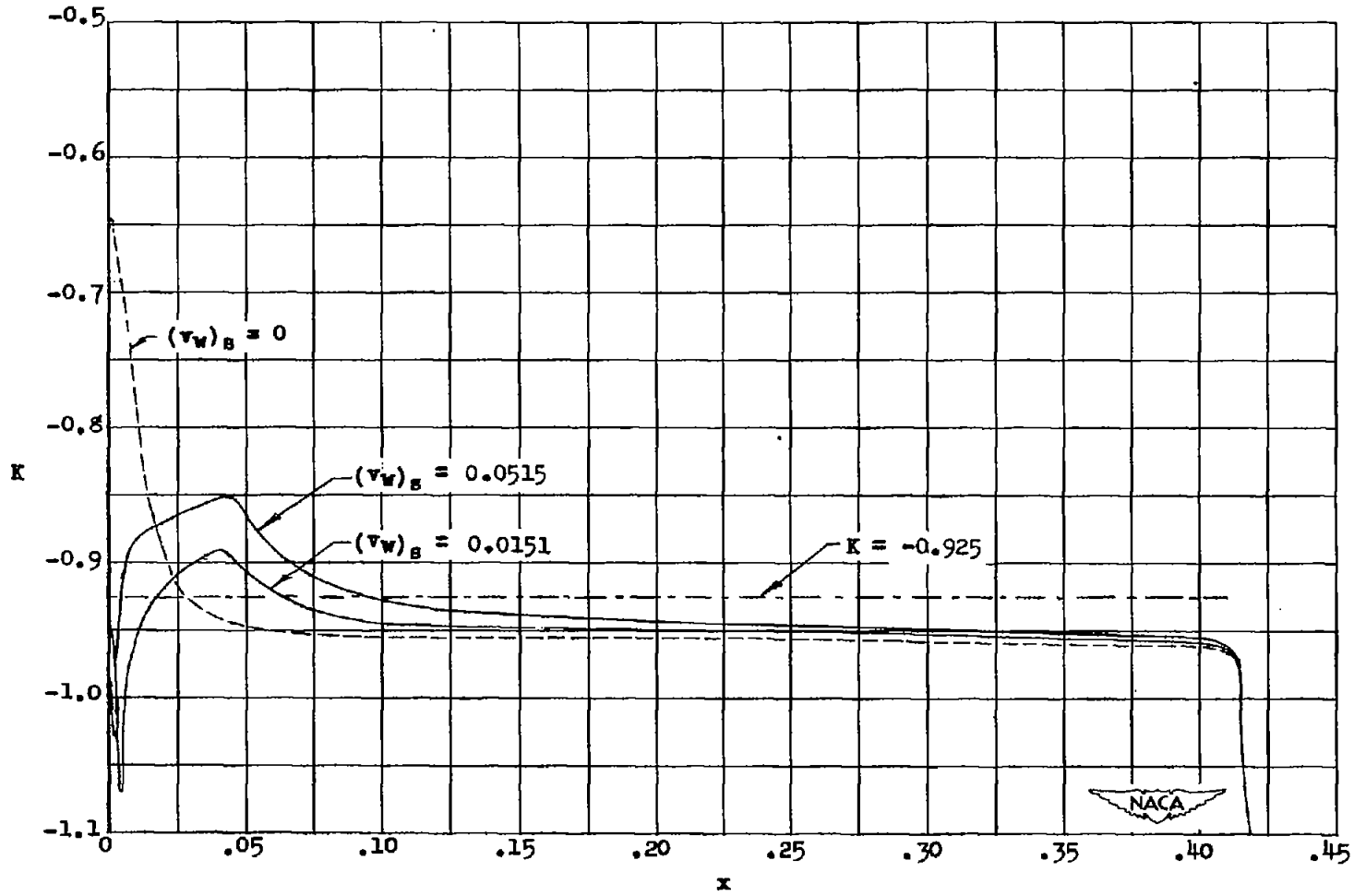

(a) Variation of velocity-profile shape parameter K with position x along surface for NACA 64A010 airfoil section at zero angle of attack for three values of $(v_w)_s$, ratio of velocity through surface at the stagnation point to free-stream velocity.

Figure 8.- Calculations for NACA 64A010 airfoil.

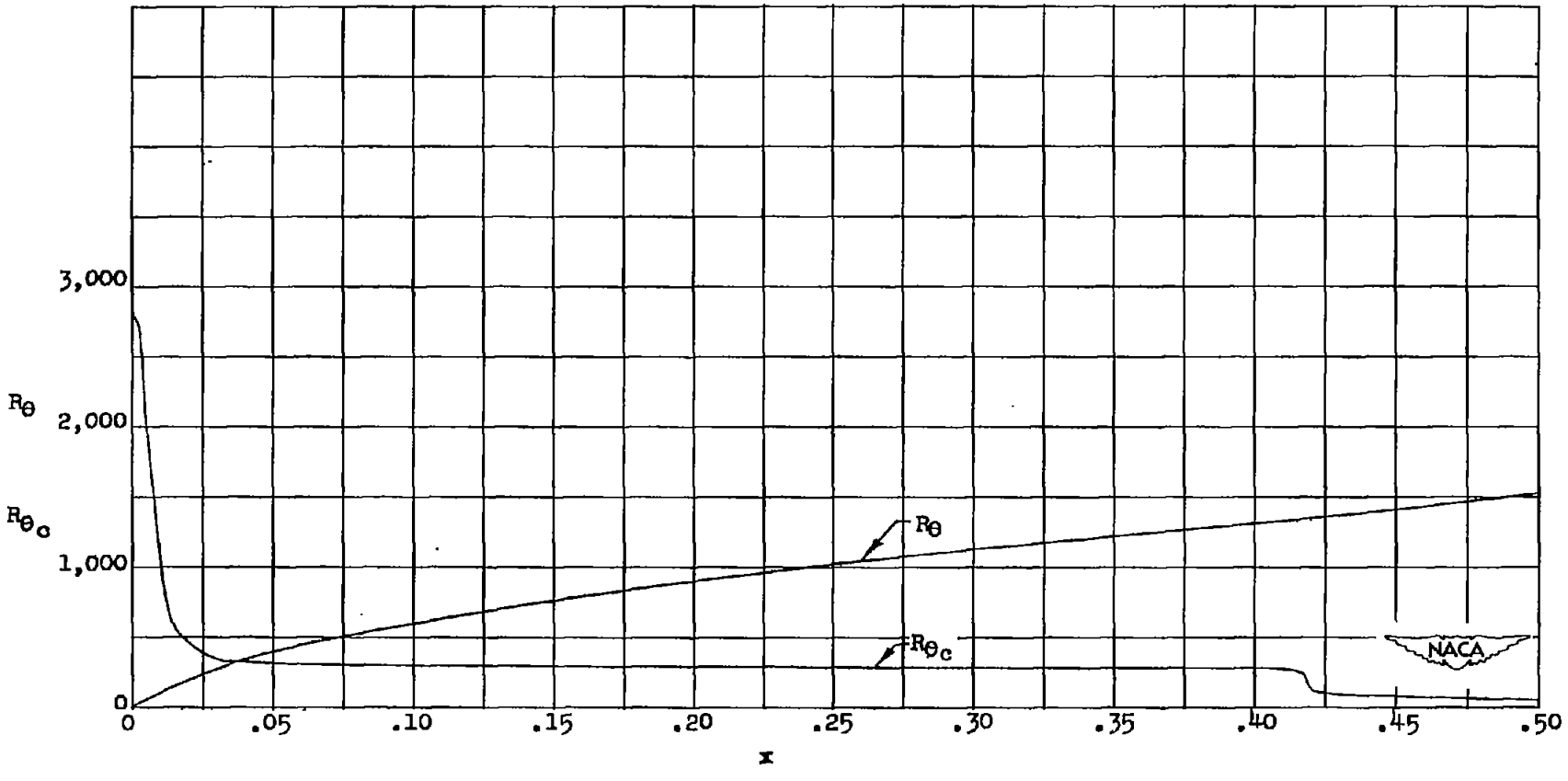

(b) Variation of boundary-layer Reynolds number R_θ and critical boundary-layer Reynolds number R_{θ_c} with position x along surface for the NACA 64A010 airoil section for no flow through surface ($v_w = 0$), a chord Reynolds number of 10^7, and zero angle of attack.

Figure 8.- Continued.

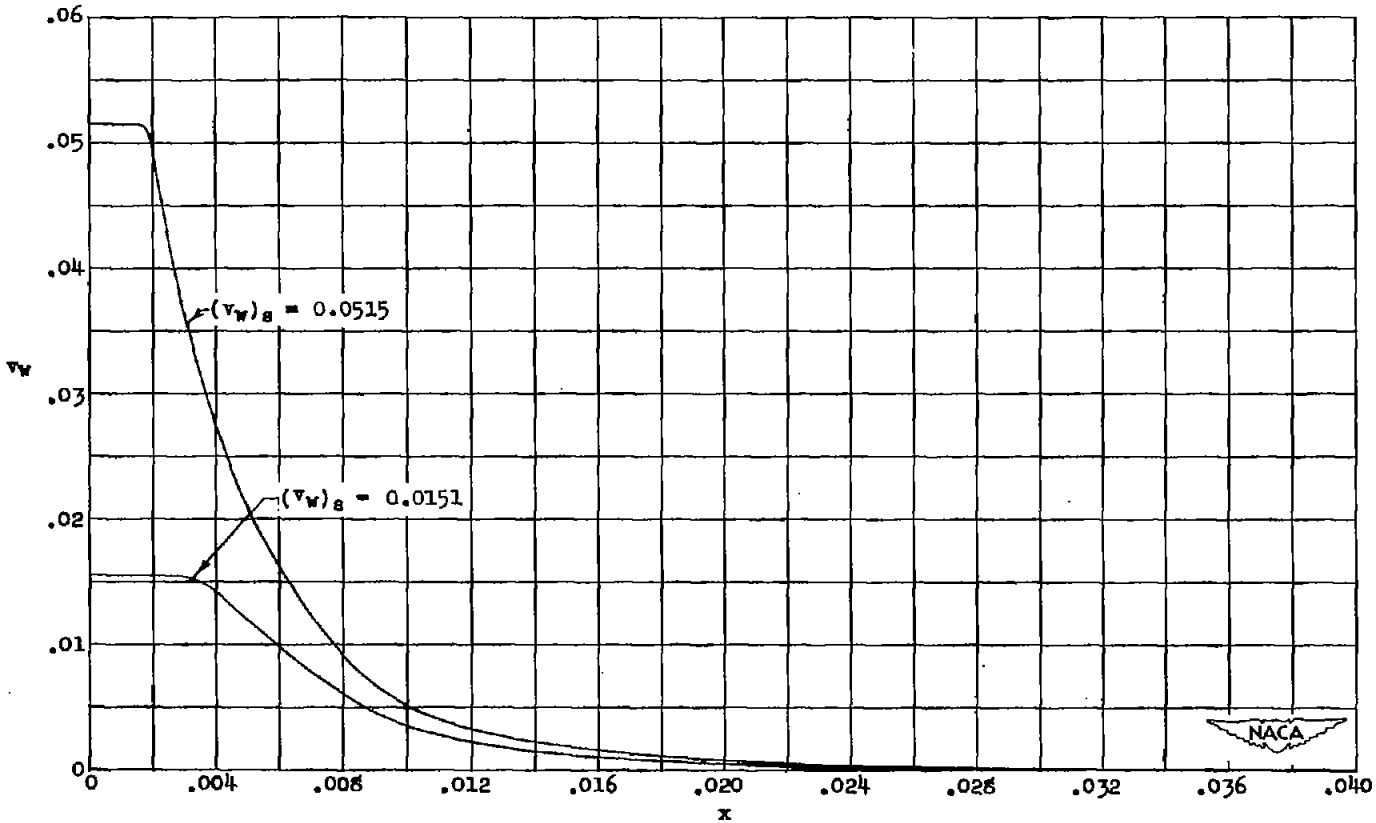

(c) Variation of v_w, ratio of velocity through surface to free-stream velocity, with position x along surface for the NACA 64A010 airfoil section at zero angle of attack, a chord Reynolds number of 10^7, and two values of $(v_w)_s$, value of v_w at stagnation point. For $(v_w)_s = 0.0515$, $\int_0^{0.04} v_w \, dx = 0.000287$ and $v_w = 0$ at $x = 0.04$; for $(v_w)_s = 0.0151$, $\int_0^{0.04} v_w \, dx = 0.000129$ and $v_w = 0$ at $x = 0.04$.

Figure 8.- Continued.

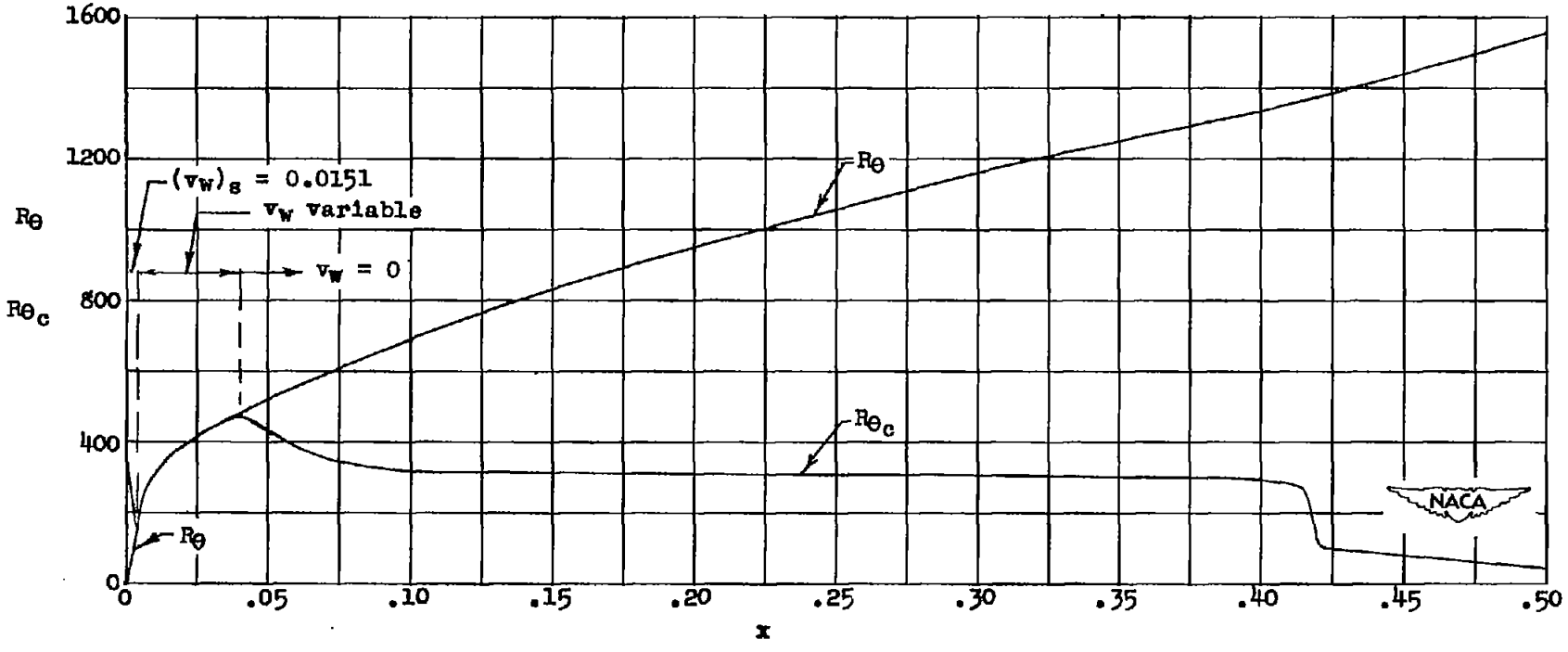

(d) Variation of boundary-layer Reynolds number R_θ and critical boundary-layer Reynolds number R_{θ_c} with position x along surface for the NACA 64A010 airfoil section for $(v_w)_s$, ratio of velocity through surface at stagnation point to free-stream velocity, equal to 0.0151, a chord Reynolds number of 10^7, and zero angle of attack.

Figure 8.- Continued.

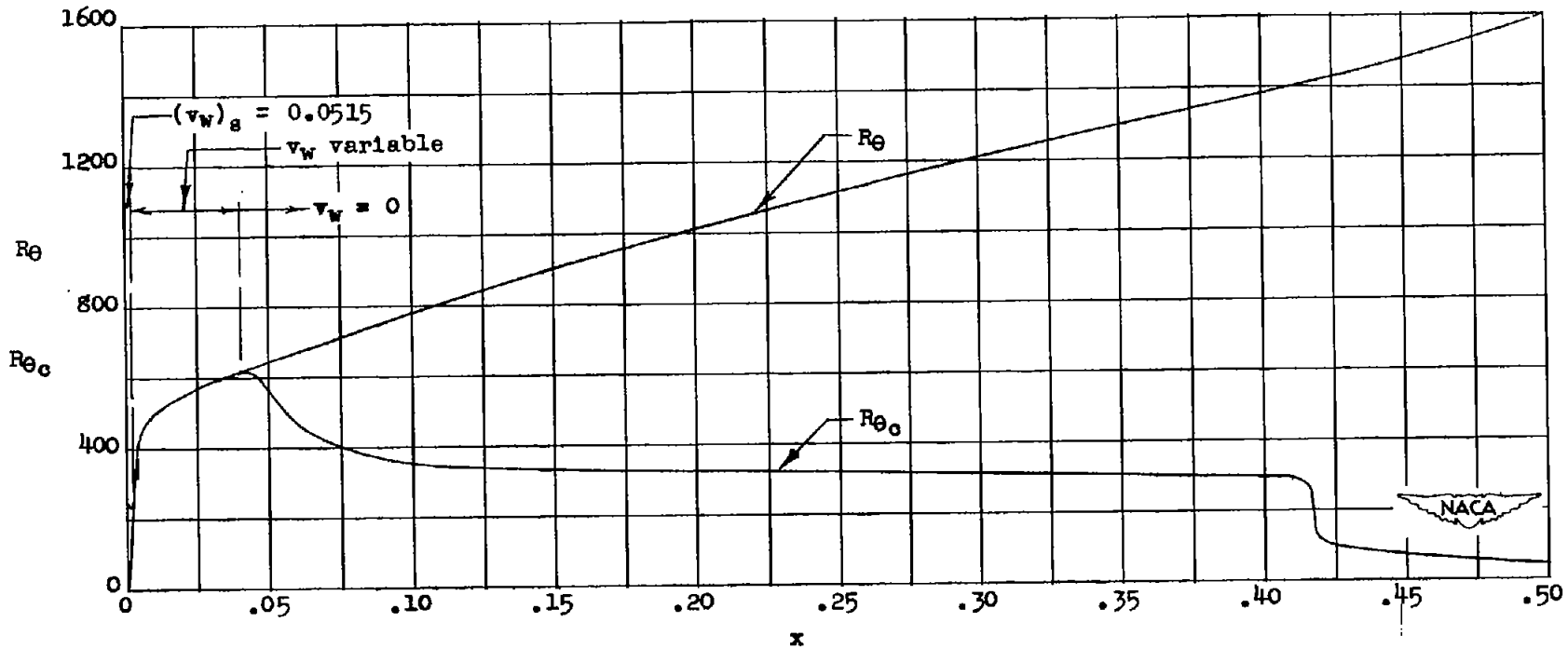

(e) Variation of boundary-layer Reynolds number R_θ and critical boundary-layer Reynolds number R_{θ_c} with position x along surface for NACA 64A010 airfoil section for $(v_w)_s$, ratio of velocity through surface at stagnation point to free-stream velocity, equal to 0.0515, a chord Reynolds number of 10^7, and zero angle of attack.

Figure 8.- Continued.

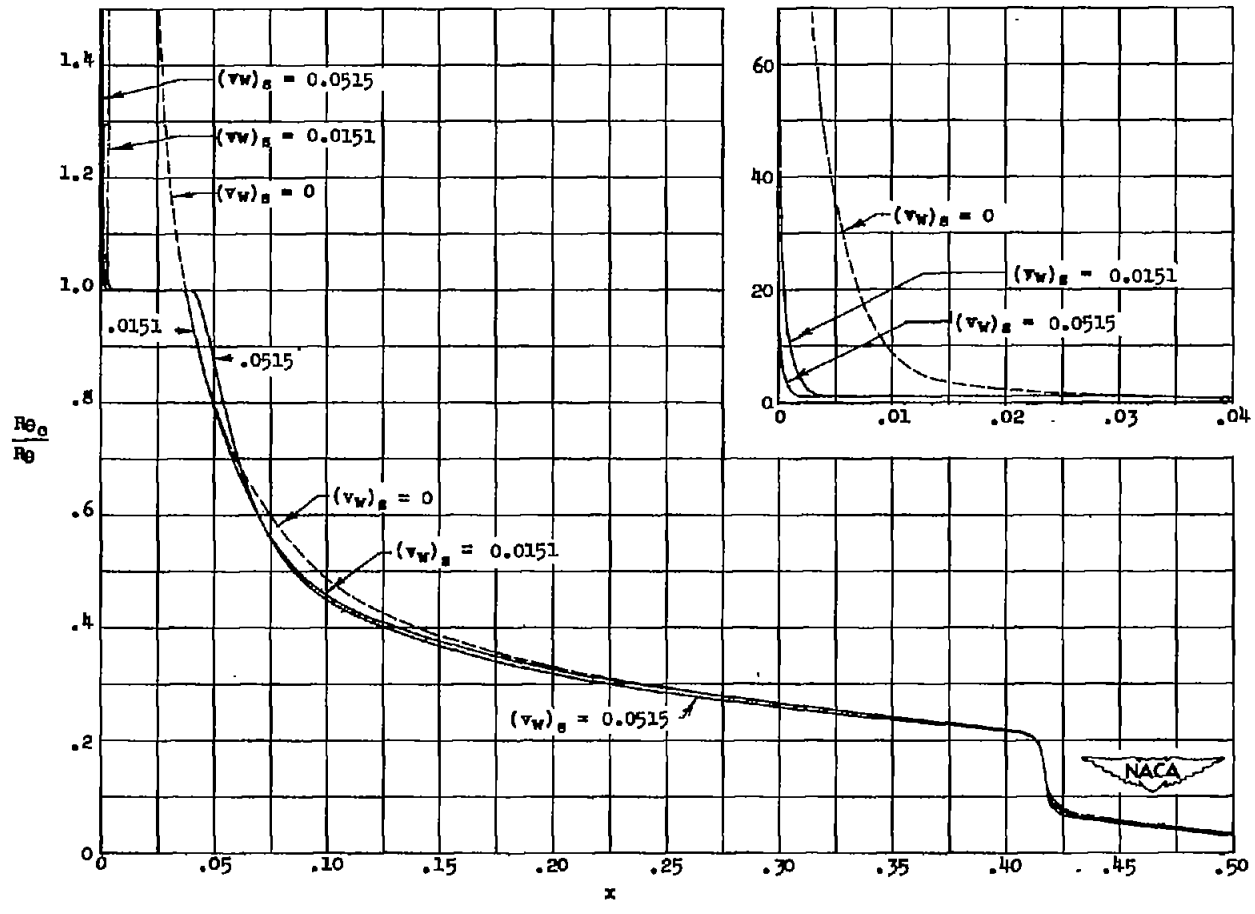

(f) Variation of the ratio of critical boundary-layer Reynolds number R_{θ_c} to boundary-layer Reynolds number R_θ with position x along the surface for the NACA 64A010 airfoil section at a chord Reynolds number of 10^7, zero angle of attack, and fixed values of $(v_w)_s$, the ratio of velocity through the surface at the stagnation point to the free-stream velocity.

Figure 8.- Continued.

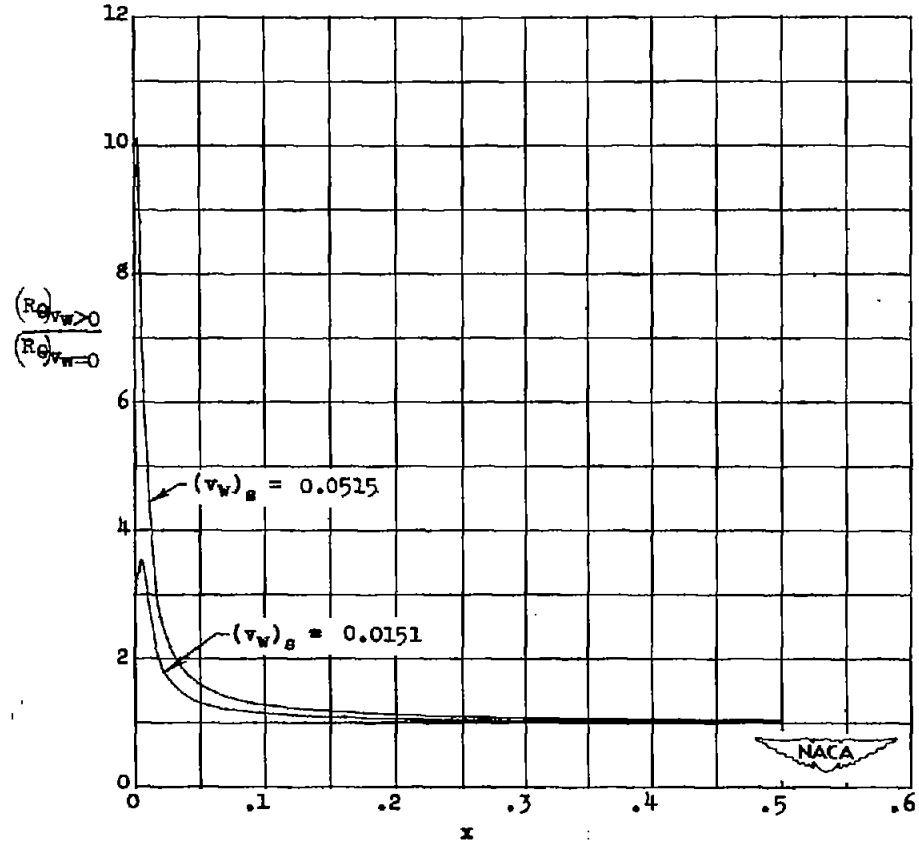

(g) Variation with position x along surface of ratio of boundary-layer thickness with blowing to thickness without blowing $\frac{(R_\theta)_{v_w>0}}{(R_\theta)_{v_w=0}}$ for NACA 64A010 airfoil section at a chord Reynolds number of 10^7, zero angle of attack, and fixed values of $(v_w)_s$, ratio of flow velocity through surface at stagnation point to free-stream velocity.

Figure 8.- Concluded.

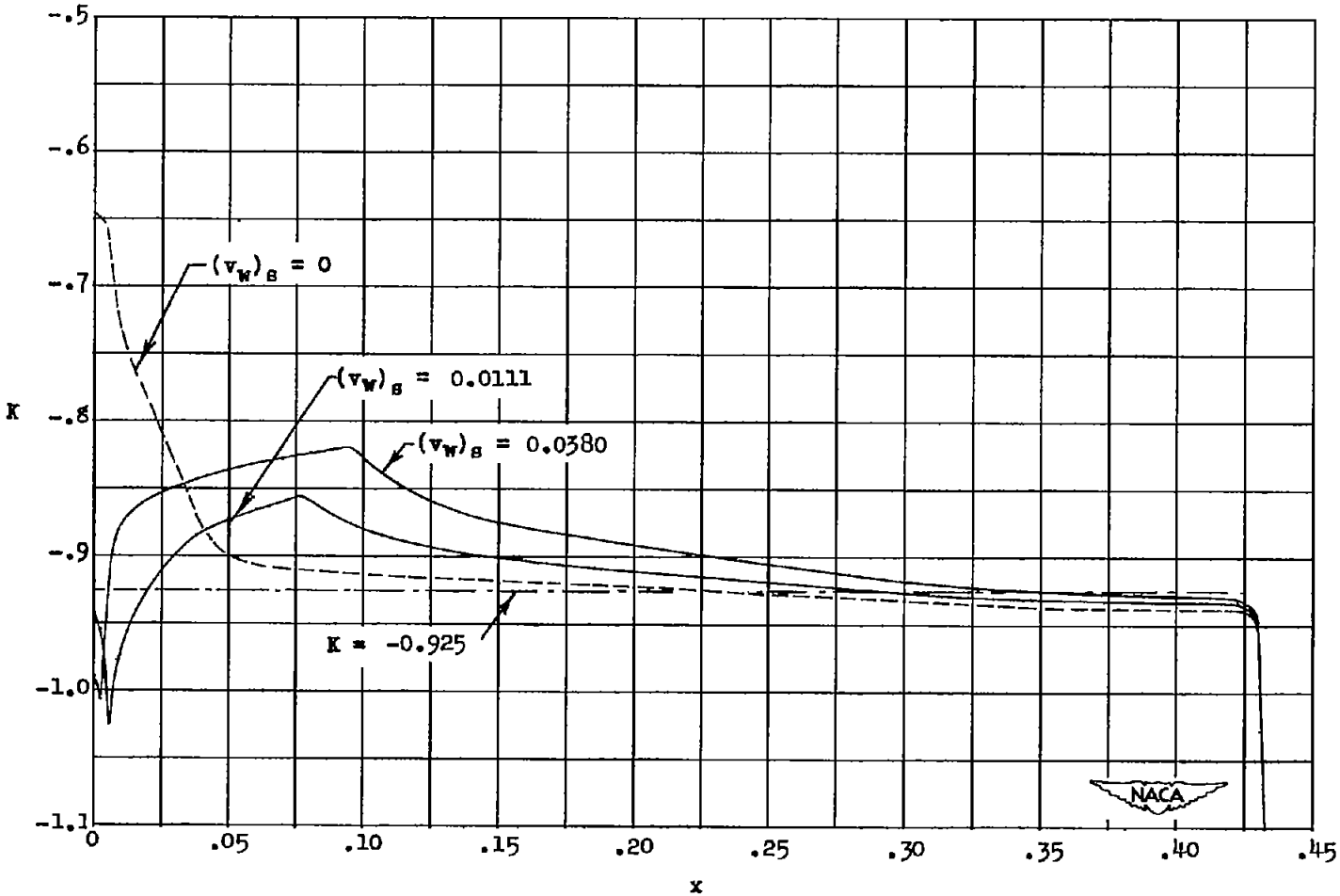

(a) Variation of velocity-profile shape parameter K with position x along surface for NACA 64_2A015 airfoil section at zero angle of attack for three values of $(v_w)_s$, ratio of velocity through surface at stagnation point to free-stream velocity.

Figure 9.- Calculations for NACA 64_2A015 airfoil.

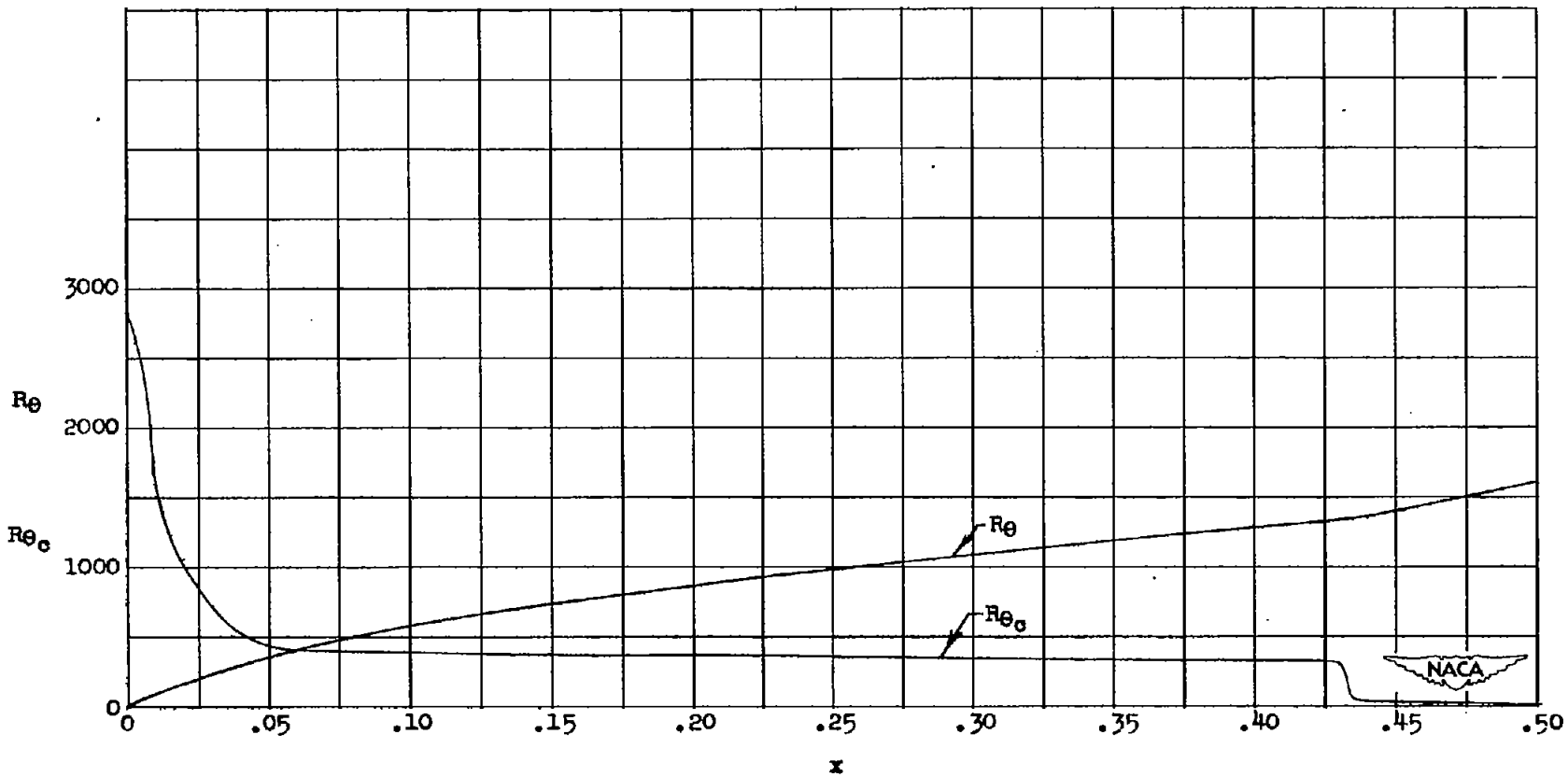

(b) Variation of boundary-layer Reynolds number R_θ and critical boundary-layer Reynolds number R_{θ_c} with position x along surface for the NACA 64_2A015 airfoil section for no flow through surface ($v_w = 0$), a chord Reynolds number of 10^7, and zero angle of attack.

Figure 9.- Continued.

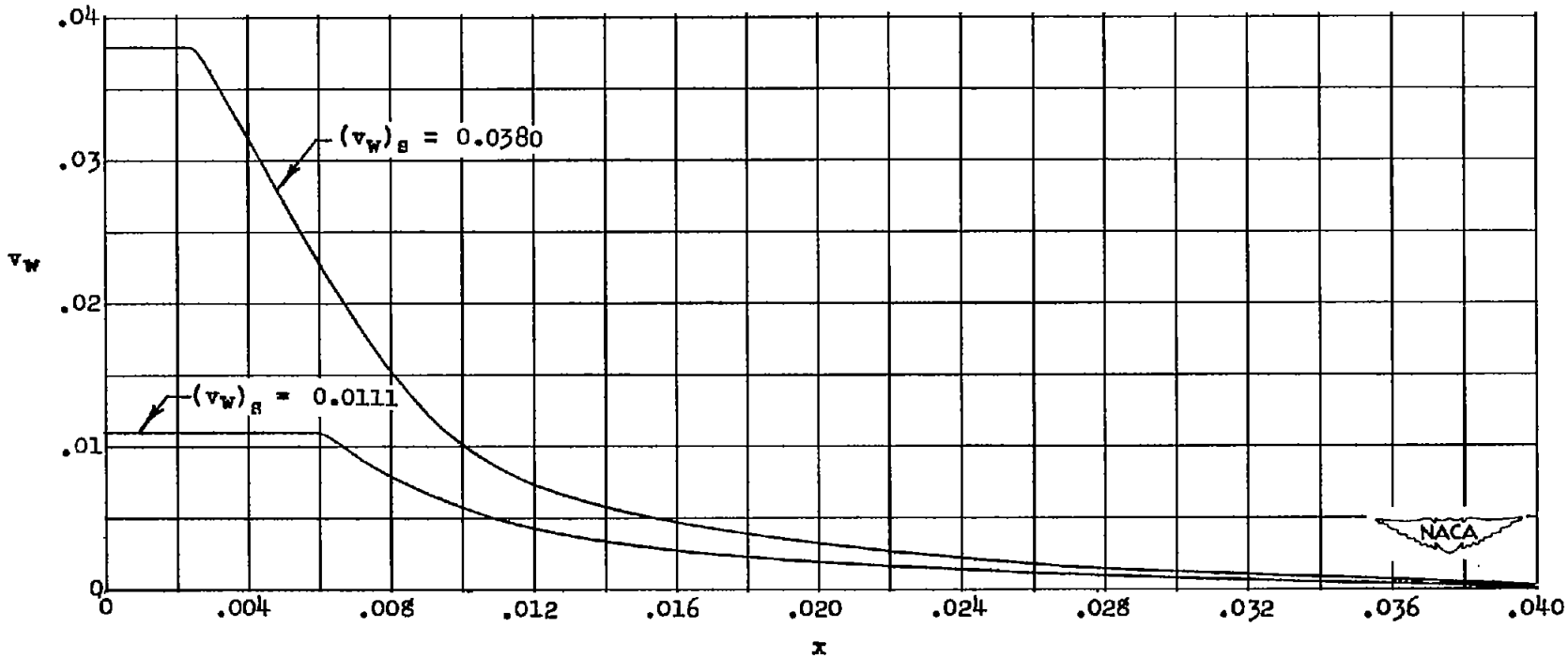

(c) Variation of v_w, ratio of velocity through surface to free-stream velocity, with position x along surface for NACA 64_2A015 airfoil section at zero angle of attack, a chord Reynolds number of 10^7, and two values of $(v_w)_s$, value of v_w at stagnation point. For $(v_w)_s = 0.0380$, $\int_0^{0.095} v_w \, dx = 0.000354$ and $v_w = 0$ at $x = 0.095$; for $(v_w)_s = 0.0111$, $\int_0^{0.075} v_w \, dx = 0.000157$ and $v_w = 0$ at $x = 0.075$.

Figure 9.- Continued.

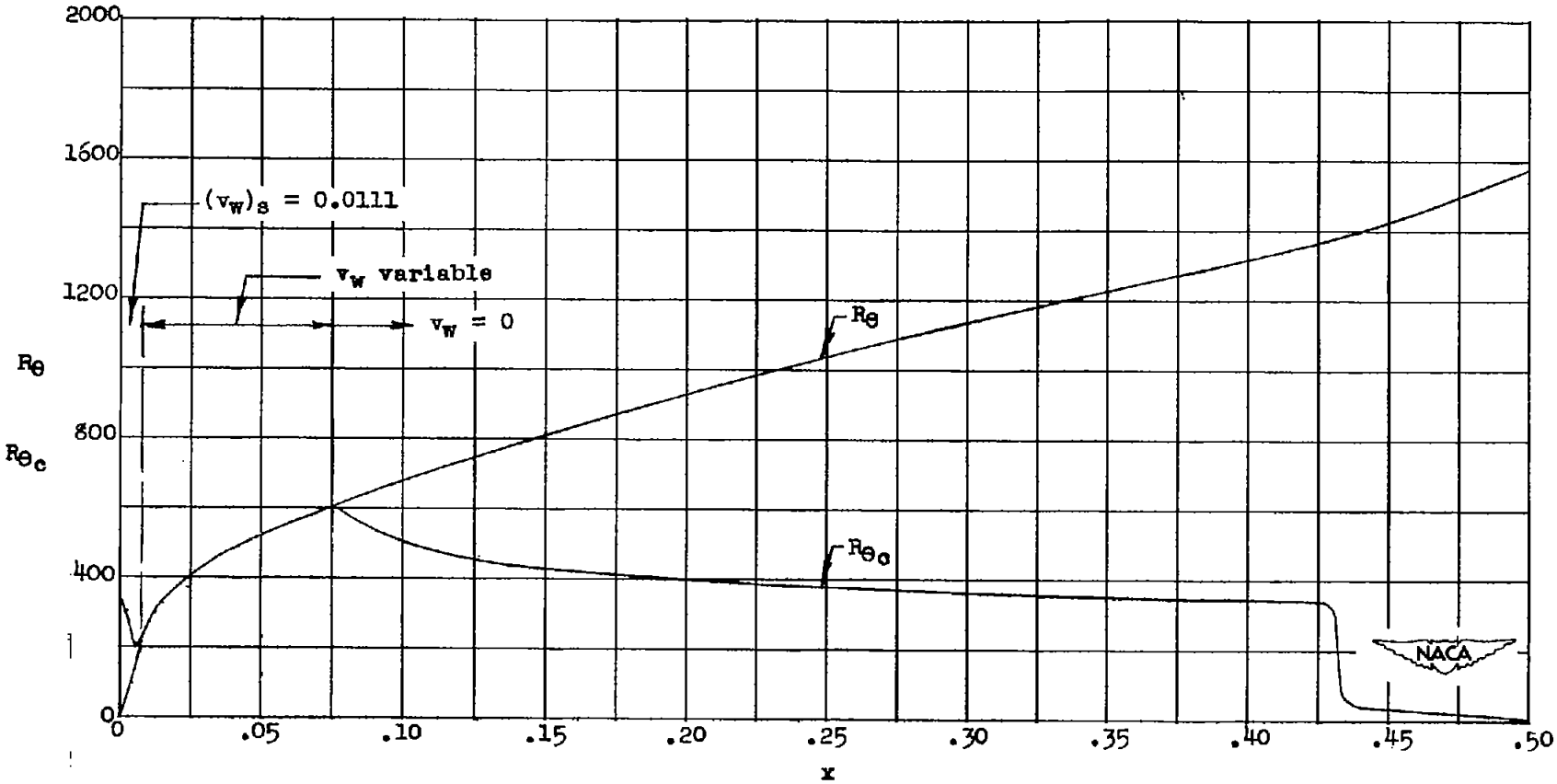

(d) Variation of boundary-layer Reynolds number R_θ and critical boundary-layer Reynolds number R_{θ_c} with position x along surface for NACA 64_2A015 airfoil section for $(v_w)_s$, the ratio of velocity through the surface, at the stagnation point to the free-stream velocity, equal to 0.0111, a chord Reynolds number of 10^7, and zero angle of attack.

Figure 9.- Continued.

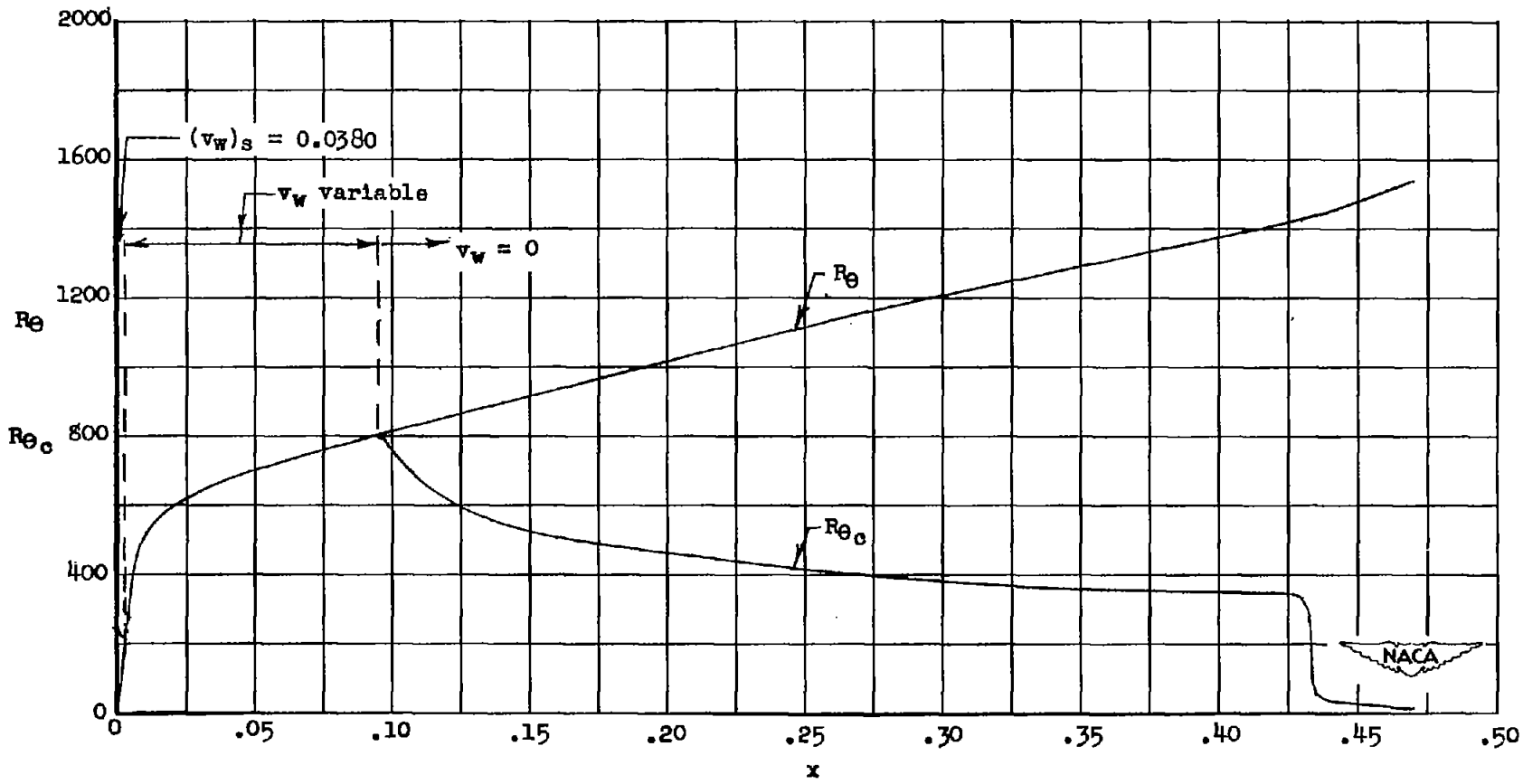

(e) Variation of boundary-layer Reynolds number R_θ and critical boundary-layer Reynolds number R_{θ_c} with position x along surface for NACA 64_2A015 airfoil section for $(v_w)_s$, ratio of velocity through surface at stagnation point to free-stream velocity, equal to 0.0380, a chord Reynolds number of 10^7, and zero angle of attack.

Figure 9.- Continued.

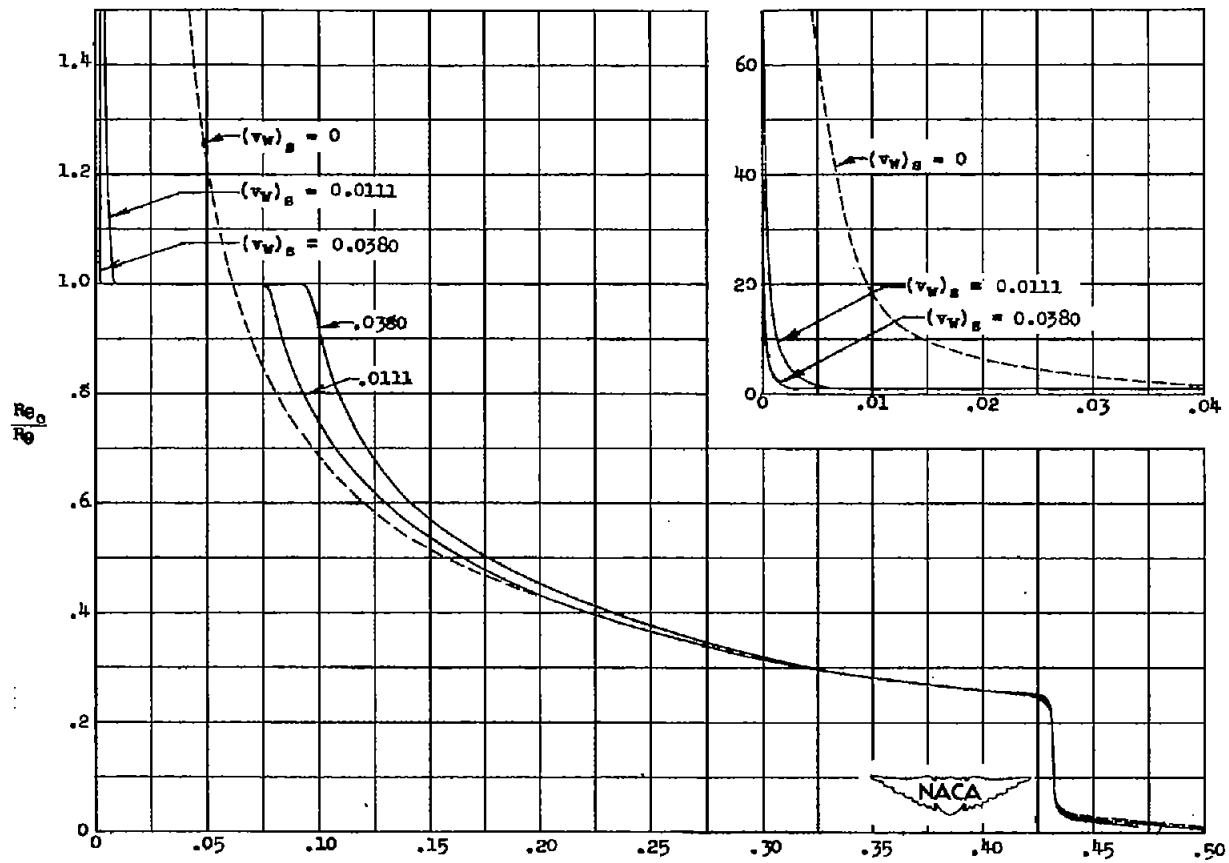

(f) Variation of ratio of critical boundary-layer Reynolds number R_{θ_c} to boundary-layer Reynolds number R_θ with position x along surface for NACA 64_2A015 airfoil section at a chord Reynolds number of 10^7, zero angle of attack, and fixed values of $(v_w)_s$, ratio of velocity through the surface at stagnation point to free-stream velocity.

Figure 9.- Continued.

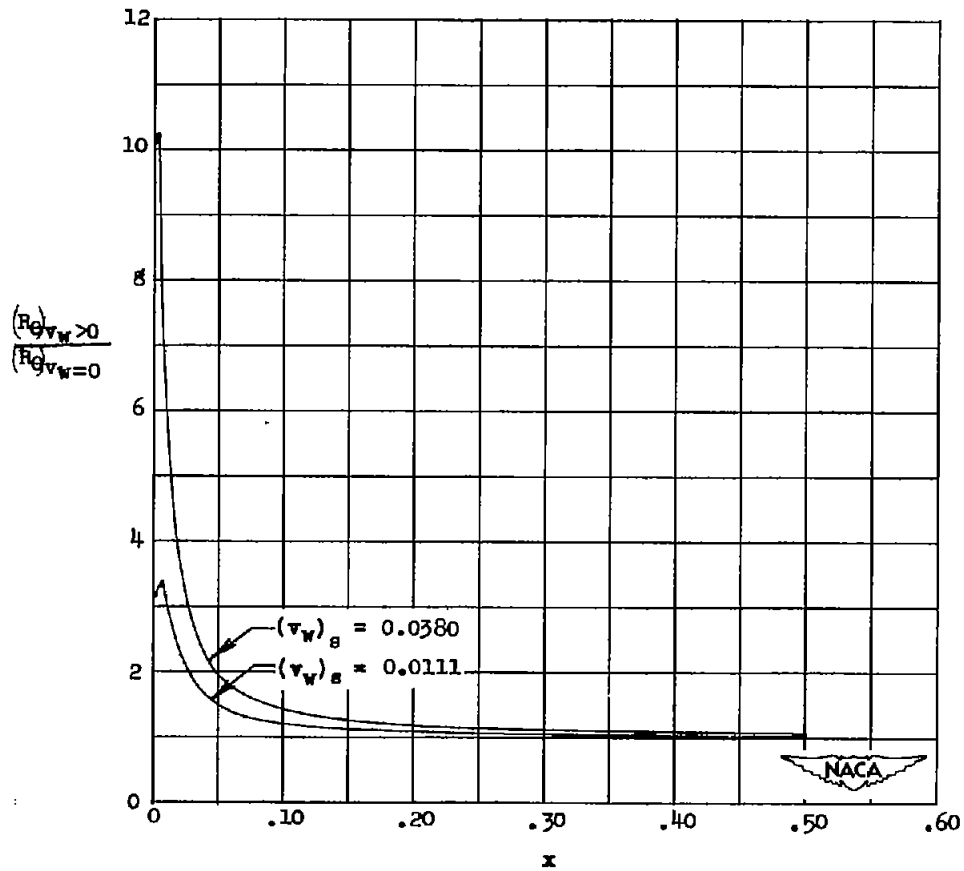

(g) Variation with position x along surface of ratio of boundary-layer thickness with blowing to thickness without blowing $\frac{(R_\theta)_{v_w>0}}{(R_\theta)_{v_w=0}}$ for NACA 64_2A015 airfoil section at a chord Reynolds number of 10^7, zero angle of attack, and fixed values of $(v_w)_s$, ratio of velocity through surface at stagnation point to free-stream velocity.

Figure 9.- Concluded.

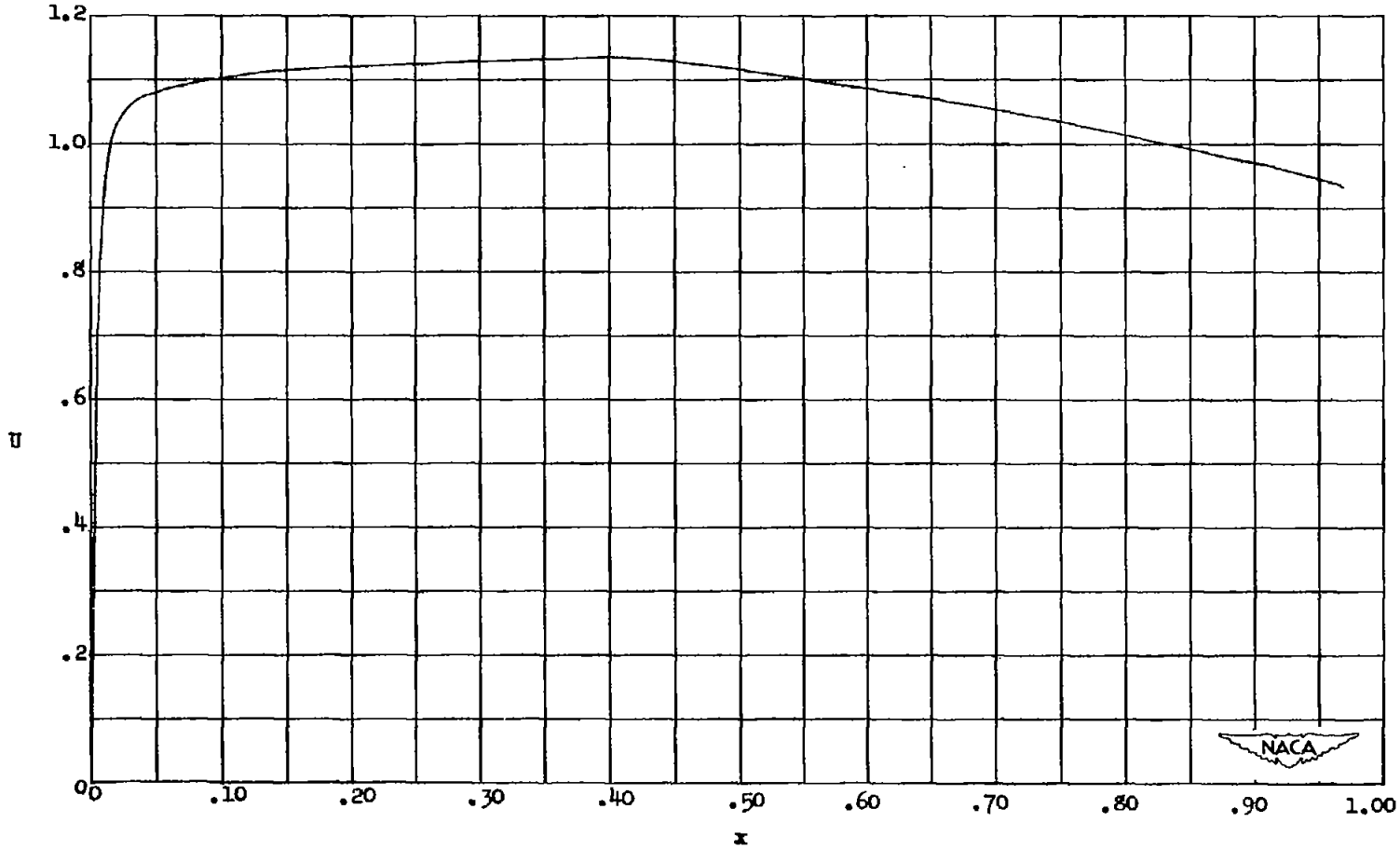

Figure 10.- Velocity distribution, U against x, for the NACA 64A010 airfoil section at $\alpha = 0^{\circ}$.

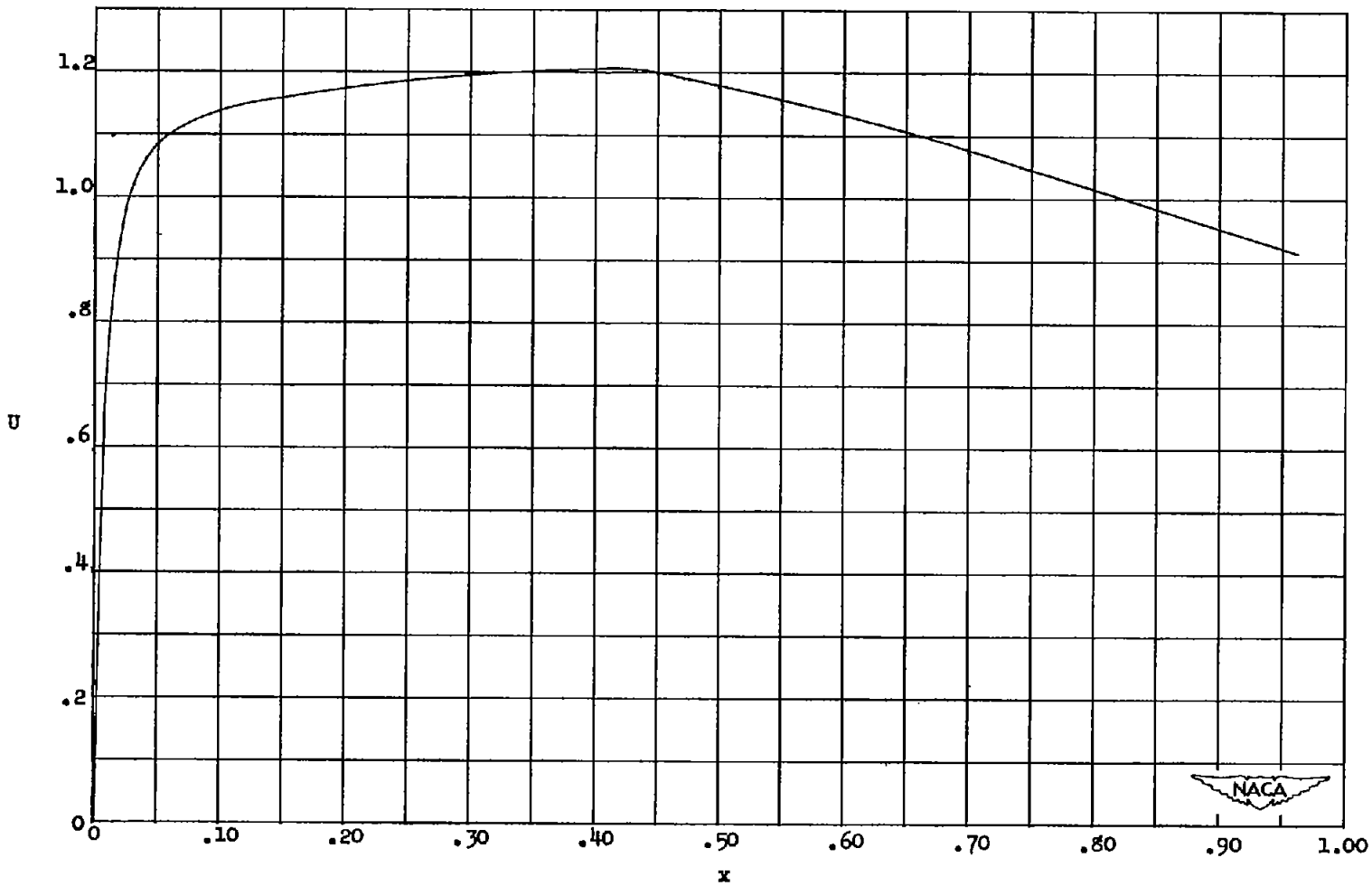

Figure 11.- Velocity distribution, U against x, for the NACA 64_2A015 airfoil section at $\alpha = 0^{\circ}$.

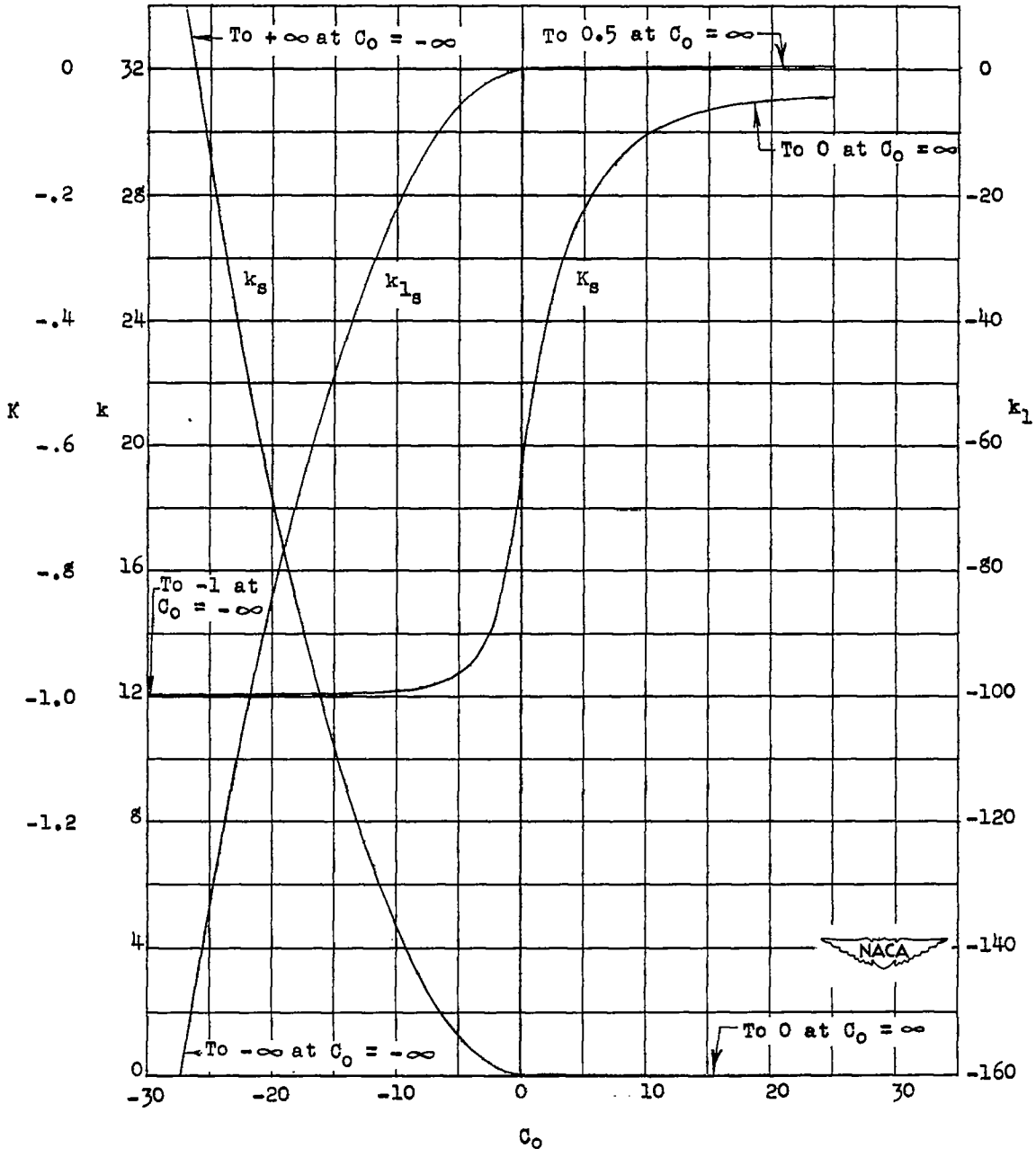

Figure 12.- Variation at stagnation point of velocity-profile shape parameter K, pressure-gradient parameter k, and parameter of flow through surface k_1, with stagnation-point parameter C_o.

$$C_o = \left(-v_w'\sqrt{\frac{R_c}{\frac{dU}{dx}}}\right)_s .$$

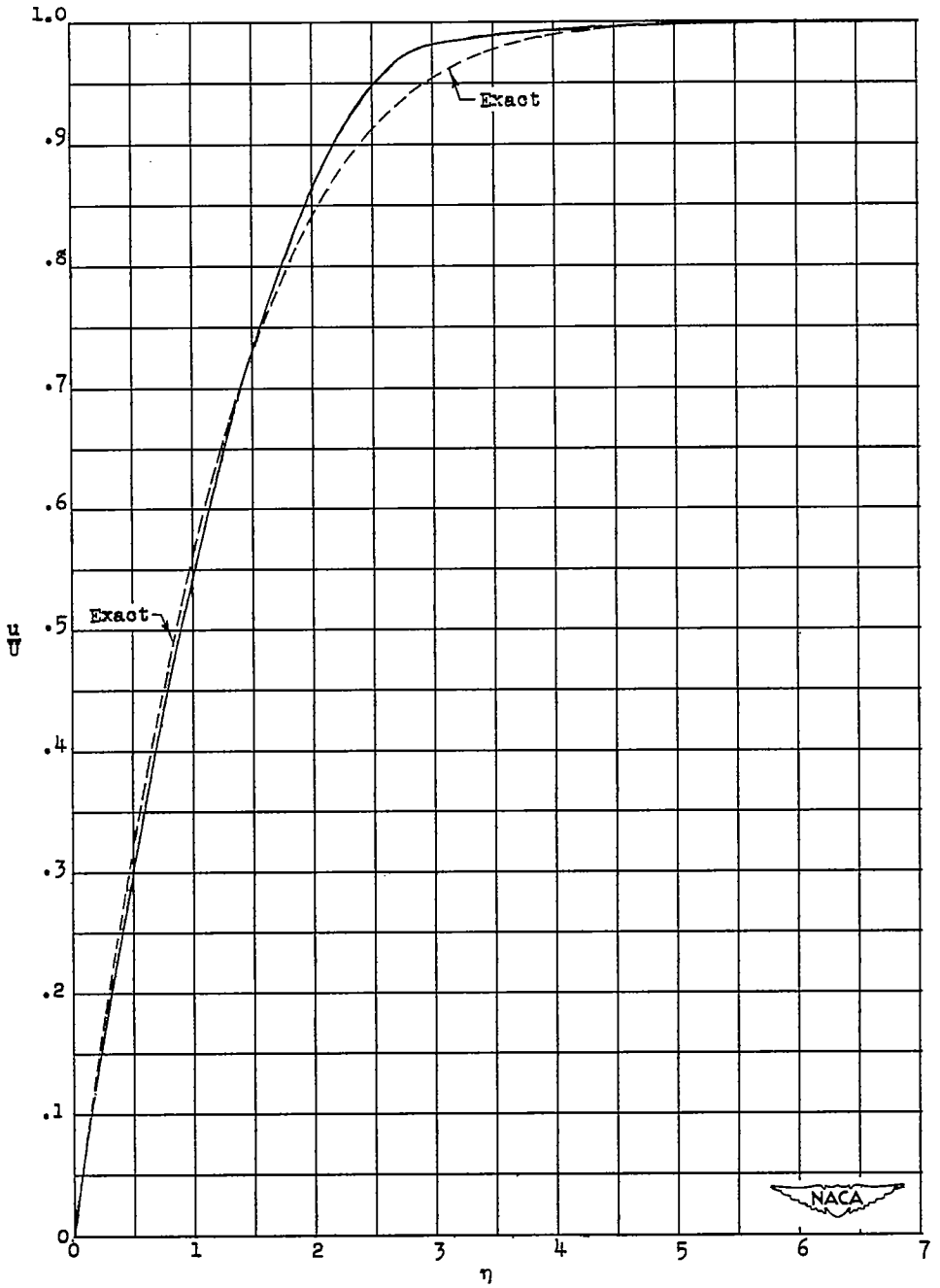

(a) No flow through the surface. $C_o = 0$.

Figure 13.- Comparison of exact and approximate boundary-layer velocity profiles at stagnation point with blowing for three values of stagnation-point parameter C_o. $C_o = \left(-v_w\sqrt{\frac{R_c}{\frac{dU}{dx}}}\right)_s$.

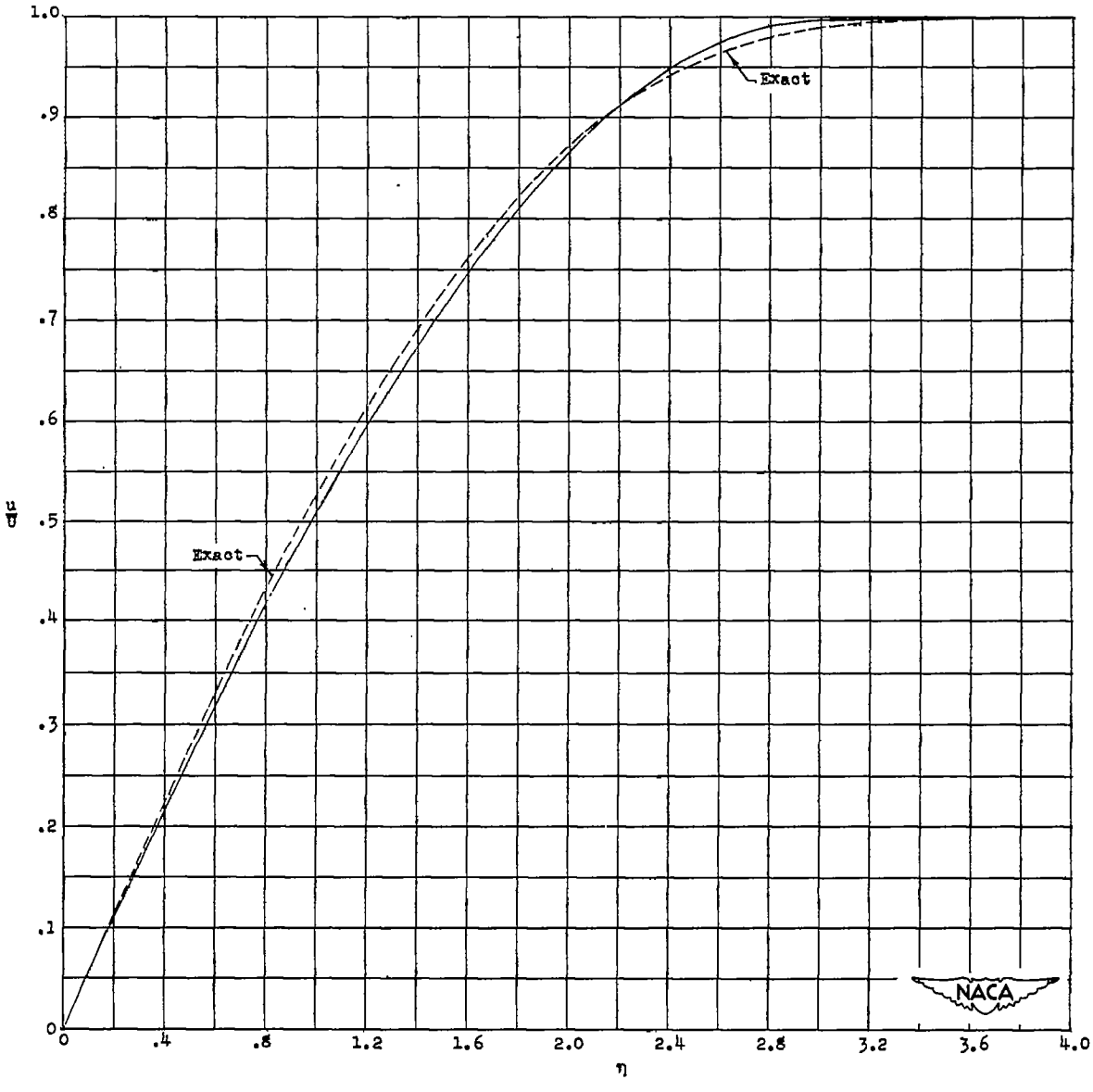

(b) Blowing. $C_o = -3.1905$.

Figure 13.- Continued.

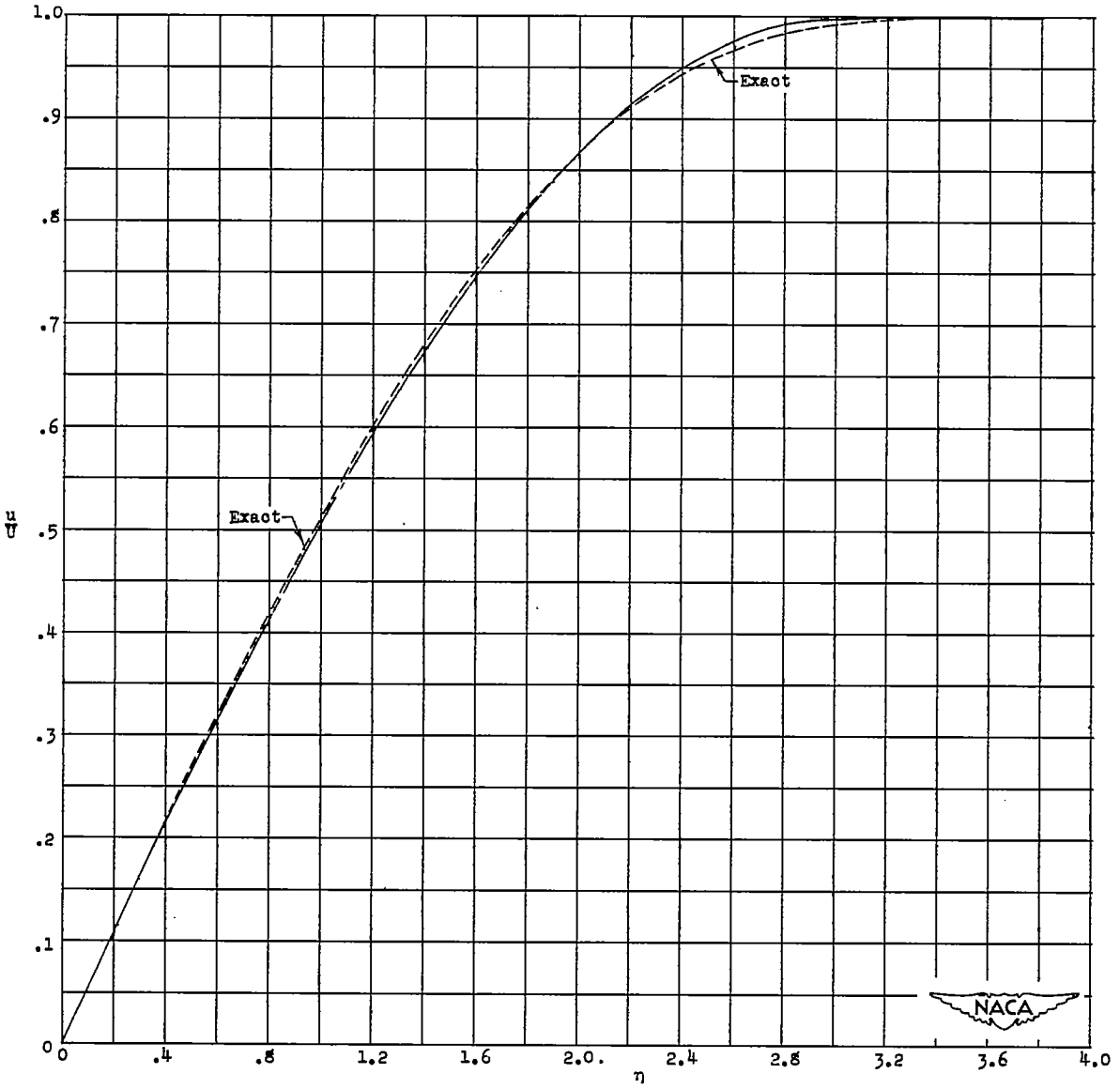

(c) Blowing. $C_o = -4.3346$.

Figure 13.- Concluded.